THE UNIVERSITY OF ADELAIDE

S-TYPE GRANITE FORMATION AT VIVONNE BAY, KANGAROO ISLAND

by SIMON F. MITCHELL B.Sc.

November, 1990

S-TYPE GRANITE FORMATION AT VIVONNE BAY, KANGAROO ISLAND

Simon F.Mitchell, B.Sc.

SI-5316-6326-III
KINGSCOTE 1:250000 SHEET
VIVONNE 1:50000 SHEET

Thesis submitted as partial fulfilment
of the Honours degree of Bachelor of Science

University of Adelaide
Department of Geology and Geophysics

October, 1990

TABLE OF CONTENTS

List of Tables and Figures

ABSTRACT

Demonstrating a genetic association between a granite and the surrounding country rock by field relationships is usually difficult. However, wave cut platform exposures at Vivonne Bay, Kangaroo Island, display a variety of granites, each of which has evolved under different but related processes. Both field relationships and geochemical analyses were used to describe the granite-migmatite association and allow the processes of formation to be assessed.

There are five major granite lithologies recognised along the Vivonne Bay section, viz; biotite granite,.garnet granite, leucocratic granite, felsic granite and porphyritic granite. Field relationships indicate that the leucocratic granite, felsic granite and garnet granite are small (<200m) intrusives, while the porphyritic granite is a kilometre scale intrusion which forms the "core" of the section. The small scale (<200m) biotite granite is intimatly associated with a biotite metasediment and granitised metasediment (or subgranite). The level of metamorphism of the metasediments is very high, reaching migmatite grade in most parts of the section, and is proportional to the proximity of the porphyritic granite core.

Geochemical analyses indicate two major trends. The first trend suggests the intrusive granites form a fractionation relationship and the second trend implies that the biotite granite is the product of partial melting of the metasediments. Mass balance modeling and an analysis of the trace element distribution reinforced the suggested trends. This study concluded that the granites at Vivonne Bay represent four different stages in melt evolution;

Stage 1: Unsegregated partial melting of the metasediments producing a subgranite

Stage 2: Metre scale segregations of partial melt from the metasediments producing a biotite granite

Stage 3: Kilometre scale pluton accumulations of biotite granite melts producing a porphyritic granite

Stage 4: Fractionation from the porphyritic granite producing a garnet granite.

1. INTRODUCTION

An understanding of the physical and chemical processes involved with the formation and segregation of granitic melts is essential to our knowledge of the genesis of continental crust. The process of granite formation occurs over long time intervals (McKenzie 1985, Wickham 1987) and at great depth within the continental crust (Hildreth 1981) and consequently cannot be observed in-situ. Therefore we are forced to infer processes from the field examples and interpret them within theoretical constraints. Most granites observed at the surface have often undergone significant migration from their source regions and show little genetic relationship with the surrounding country rock. However, some granites, particularly S-type granites, illustrate genetic relationships with the rocks they are emplaced in. These examples provide an excellent environment to test physical and chemical models for the generation and segregation of granites.

The granites at Vivonne Bay on Kangaroo Island, South Australia, show field and geochemical relationships with the enclosing metasediment, from pluton-scale accumulations to granitisation in-situ from migmatite. In this thesis I aim to demonstrate the following points;

(1) at Vivonne Bay there are several granite types, each of which has evolved in response to different processes, and

(2) the processes involved include: (a) diapiric ascent of a kilometre scale pluton granite body (porphyritic granite) after crustal melting; (b) coalescence of small melt fraction segregations (garnet granite, leucocratic granite, pegmatite and felsic granite) that evolved from the diapir and intruded the metasediment as dykes up to 200 meters in length; and (c) diapir induced melting of the metasedimentary roof rocks, resulting in a granite (biotite granite and subgranite) segregated on scales of the order of metres.

2. LOCATION, REGIONAL GEOLOGY AND PREVIOUS WORK

The Vivonne Bay granite-migmatite sequence is exposed as a wave-cut platform, between Point Ellen, Vivonne Bay, and westward for approximately 4.5 kilometres toward Cape Kersaint on the south coast of Kangaroo Island (Locality figure, main map). Kangaroo Island contains the most southerly exposures of the Adelaide Fold Belt. On the north coast there are lower Cambrian sandstones, limestones and conglomerates while lower Cambrian Kanmantoo Group quartzites and schistose slates occur on the south coast (Milnes *et al.* 1977). The latter is intruded by a number of Palaeozoic granites and granodiorites particularly well exposed along the South coast (Limb 1975). The interior of the island is covered by a thin sequence of Quaternary sediments with some rare exposures of the Kanmantoo Group mainly confined to a few river channels (Milnes *et al.* 1977). These examples are highly weathered and poorly exposed, hence this study was almost entirely confined to the excellent exposures along the wave-cut platform.

Previous studies on Kangaroo Island have concentrated on Dudley Peninsular and along the north coast near Emu Bay (Milnes 1973, Daily *et al* 1979, Jenkins 1989). The granite exposed at Cape Kersaint has been described by various authors and equated with the Cape Willoughby or Encounter Bay granites (Limb 1975, Milnes *et al.* 1977). The intrusive granites are described as syn-orogenic biotite foliated granites with opalescent blue quartz and distinctive megacrysts of plagioclase, potassium feldspar and quartz (Milnes *et al.* 1977). The nature of the granite-Kanmantoo group contact at Cape Willoughby and Encounter Bay is concordant with bedding, with a suggested emplacement mechanism of active stoping and enforced intrusion along bedding planes (Milnes *et al.*, 1977).

Ages determined for the area include a 519+/-6 Ma (Milnes *et al.*, 1977) Rb/Sr age of a pegmatite at Point Ellen. Milnes *et al.*, 1977, also determined a K/Ar muscovite age of 485 Ma from the same pegmatite. The Cape Kersaint granite, the main granite body in the Vivonne Bay region, has been dated at 493+/-5 Ma from Rb/Sr data (Milnes 1973).

Only a limited amount of work has been done on the Vivonne Bay migmatite-granite. Limb, (1975), completed some geochemical analyses of the Kangaroo Island granites and described the migmatite as granitised Kanmantoo metasediment. Clarke and Powell, (1989), interpreted the migmatite, with its elongation lineation and contrasting metamorphic grade with the surrounding Kanmantoo schists, as locally exposed basement. However this thesis presents evidence which suggests that the migmatitic metasediments represent the metamorphosed aureole of Kanmantoo Group rocks adjacent to the Cape Kersaint granite.

3. LITHOLOGICAL DESCRIPTION

For the purpose of this thesis I have distinguished twelve lithologies, excluding the cover sequence, along the Vivonne Bay section. These include biotite, quartz-biotite, muscovite-biotite, biotite-quartz and quartz metasediments, subgranite, biotite granite, garnet granite, leucocratic granite, felsic granite, porphyritic granite and pegmatite. The cover sequence is composed of a shelly layer and calcrete as well as Quaternary soils. These lithologies are illustrated in the main map, with the Vivonne Bay section being divided into sequences, three of these displaying diagnostic melting relationships (sequences 1, 3, 5, see main map).

The general field relationships between the lithologies are summarised in figure [1]. Most of the granites, including the biotite granite, garnet granites and subgranite, occur at the margin of a porphyritic granite, the syn-orogenic "granodiorite" of Milnes *et al.* , 1977, that forms the core of the section at the western end of the field area. The scale of the granite dyke bodies decreases eastward towards Point Ellen, as does the degree of migmatisation of the metasediments and their relative proportion of the residual minerals biotite and muscovite. The exception to this occurs at Point Ellen itself, where there are high levels of migmatisation associated with several phases of early felsic granite and late pegmatite intrusive dykes. The metasediment is subdivided on the basis of changes in general mineralogy from the pluton margin to Point Ellen where the relative proportion of quartz increases.

3.1. THE GRANITES

There are seven distinctive granite types in the field area. As will be seen, their field relationships (main map, and figure [1]) and geochemical signatures demonstrate that they represent various degrees of melting and stages in the evolution of the intrusive porphyritic granite aureole.

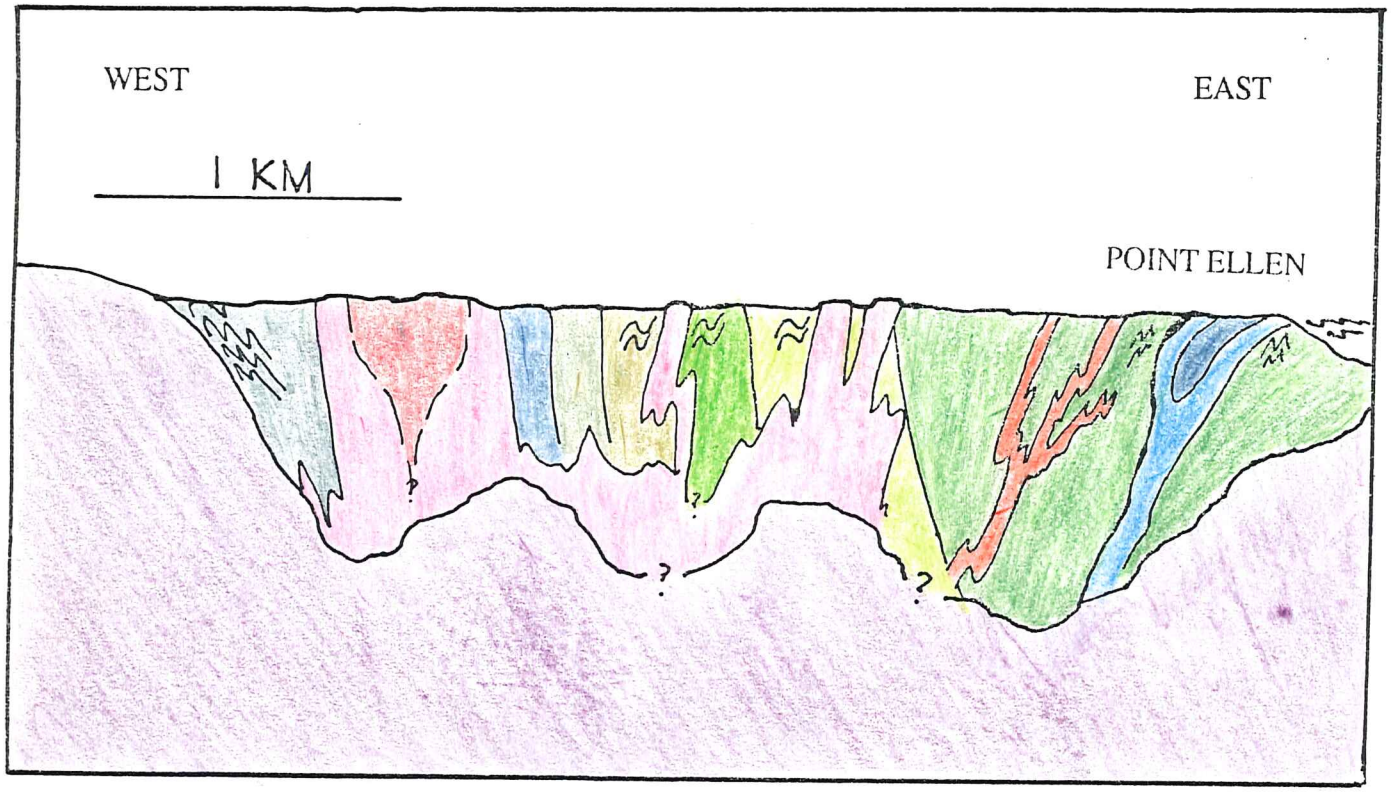

METASEDIMENT

QUARTZ

MUSCOVITE-BIOTITE

BIOTITE-QUARTZ

QUARTZ-BIOTITE

BIOTITE

SUBGRANITE

BIOTITE GRANITE

FELSIC GRANITE

GARNET GRANITE

LEUCOCRATIC GRANITE

PORPHYRITIC GRANITE

PEGMATITE

FIGURE [1] GENERALISED RELATIONSHIPS BETWEEN THE VIVONNE BAY LITHOLOGIES

TABLE 1. SELECTED MICROPROBE ANALYSES OF MINERAL COMPOSITIONS FROM THE VIVONNE BAY MIGMATITE-GRANITE

SAMPLE	1	2	3	4	5	6	7	8	9
Biotite composition									
SiO2	34.38	33.95	33.88	34.63	34.56	33.68	34.44	34.14	34.34
TiO2	3.23	3.9	0	2.21	2.2	2.97	2.79	2.29	2.95
Al2O3	16.55	17.38	18.31	18.29	18.71	16.69	17.79	17.96	17.02
FeO	20.2	23.52	17.41	18.83	17.69	20.83	18.42	18.72	20.59
MnO	0.3	0	0.7	0.27	0.18	0.29	0	0.13	0.14
MgO	8.68	4.73	10.06	9.27	10.1	7.65	9.53	8.88	7.82
CaO	0	0.12	0	0	0	0	0	0	0
K2O	9.4	9.67	7.99	9.62	9.04	9.78	9.61	9.5	9.67
Na2O	0.38	0.22	0.31	0.15	0.3	0	0.3	0.39	0.24
Mg/Mg+Fe	0.30	0.16	0.37	0.36	0.36	0.27	0.34	0.32	0.28
Total (%)	93.19	93.59	88.67	93.26	92.77	91.88	92.93	92.01	92.86
Plagioclase feldspar compositions									
SiO2	60.42	65.96	66.26	60.43	59.44	60.98	60.77	59.11	65.97
Al2O3	24.75	20.65	20.25	24.67	25.14	23.9	24.32	24.85	20.78
CaO	6.58	1.85	1.64	6.72	7.14	5.97	6.42	7.3	1.53
K2O	0.14	0.49	0.26	0.19	0.13	0.3	0.27	0.18	0.25
Na2O	7.78	10.24	10.24	7.77	7.51	8.03	7.79	7.37	10.47
P2O5	0	0.35	0	0	0	0.11	0	0	0
Total (%)	99.66	99.6	98.65	99.78	99.36	99.35	99.58	98.81	99
Approximate proportions of minerals (%)									
Quartz	30	25	25	30	20	15	40	30	30
Plagioclase	25	35	30	25	35	25	25	25	25
K-feldspar	20	30	35	15	10	10	10		28
Biotite	15	2	2	25	30	35	20	30	15
Muscovite	8	2	6	5	5	15	5	15	2
(1) Primary	2	1	2	1	1	10		5	1
(2) Secondary	6	1	4	4	4	5	5	10	1
Garnet		5							
Sillimanite		1						1	
Chlorite	2	1	2						
Tourmaline		1	1					1	
Beryl			1						

Samples: (1) Porphyritic granite, Vivonne Bay (929-07)
(2) Garnet granite, Vivonne Bay (929-11)
(3) Leucocratic granite, Vivonne Bay (929-32)
(4) Biotite granite, Vivonne Bay (929-38)
(5) Subgranite, Vivonne Bay (929-26)
(6) Biotite metasediment, Vivonne Bay (929-37)
(7) Quartz-Biotite metasediment, Vivonne Bay (929-35)
(8) Biotite-Quartz metasediment, Vivonne Bay (929-04)
(9) Felsic Granite, Vivonne Bay (929-49)

PORPHYRITIC GRANITE

The porphyritic granite occurs as a series of plutonic intrusions along the South coast of Kangaroo Island and it is located at the Western end of sequence 1 (main map), where it is exposed as light brown-grey tors weathering in spherical sheets. In handspecimen the porphyritic granite is medium to coarse grained with approximately 1cm sized megacrysts of plagioclase, potassium feldspar and quartz. The matrix is composed of quartz (30%), plagioclase (25%), potassium feldspar (20%), biotite (15%), muscovite (8%) and minor amounts of chlorite (2%). Biotite is typically titanium and iron rich (TiO_2 ~ 3.2%, Total Fe_2O_3 ~ 20%) while plagioclase feldspar has high calcium content (CaO ~ 6.5, see Table 1).

The porphyritic granite contact with the metasediment is poorly exposed, but it shows a gradational contact with a subgranite (see next lithology) on the scale of approximately one metre. A weak foliation evident at the plutons margins, is concordant with the long axis of the metasediment xenoliths and is interpreted as a flow foliation. Xenoliths can be divided into two types; small spherical (< 20 cm) xenoliths with magmatic igneous textures and small (< 50 cm) elongate metasediment xenoliths with a strong foliation .

SUBGRANITE

The subgranite has both a metasedimentary character, with a strong penetrative foliation and easily distinguishable grains that are not interlocked in a granitic texture, and migmatitic character with layers that are clearly centimetre sized leucosomes of interlocking grains of quartz and feldspar (Plate 1 photo d). Most examples show these granitised layers as being trapped within the foliated layers, with a few layers joining up into more homogeneous regions suggesting that the process of segregation was still actively taking place. The subgranite is dominated by the minerals biotite (30%), muscovite (5%) and plagioclase (35%), but also contains significant quartz (20%) and K-feldspar (10%), the latter being confined to the melt layers which implies that it is a product of the melting. Biotite has relatively low titanium (TiO_2 ~ 2%) and iron ($Fe_2O_{3(T)}$ ~17.5%) compared with the granites (Table 1). The plagioclase feldspar compositions are very high in calcium (CaO~7.1%)

The subgranite in places shows gradational contacts with the granodiorite and elsewhere is surrounded completely by garnet granite or leucocratic granites (sequence 1, main map). Futhermore, the subgranite is in gradational contact with the biotite granite, suggesting a genetic relationship, and representing an intermediate stage between metasediment and melt, an interpretation which is investigated further in the geochemical section (section 6).

BIOTITE GRANITE

The biotite granite is a dark grey, strongly foliated, medium grained quartz-biotite-plagioclase-K-feldspar granite, containing abundant xenoliths of biotite metasediment and quartz-biotite metasediment, ranging in size from centimetres to meters. The long axis of the xenoliths are flattened in the plane of the foliation, with the rims of the xenoliths having biotite accumulations of 2-3cm in thickness.

The biotite granite has a direct concordant contact with the biotite metasediment, quartz metasediment and subgranite (sequence 1 and 5, main map). The biotite compositions are relatively low in titanium (~2.2%) and iron (~18.8%) compared with the porphyritic granite and garnet granite, but are similar to the subgranite and other metasediments (Table 1). The biotite granite is superficially similar to the porphyritic granite, with megacrysts of plagioclase and K-feldspar, but lacks dominant quartz megacrysts, the foliation is much more penetrative and it has abundant centimetre sized lenses of biotite accumulations.

GARNET-GRANITE

The garnet granite is leucocratic and weakly foliated, outcropping only along sequence 1 (main map). Sparsely distributed accumulations of garnet up to 10 cm in diameter are the most striking mineralogical feature. Joining the separate aggregations may define a line or trail suggesting confinement to cross-cutting veins. The garnet granite is feldspar rich (~70%), containing both plagioclase and potassium feldspar in approximately equal proportions, in addition to quartz (25%), muscovite (2%) and minor amounts of tourmaline(< 1%). The garnet granite contains rare titanium and iron rich biotites which are comparable with the biotites of the

(CaO ~ 1.8%) which is typical of the granite dyke bodies such as the leucocratic granite and felsic granite.

The garnet granite lacks significant numbers of small scale (< 50cm) xenoliths but does have a number of large scale (1m - 15m) xenoliths of subgranite and biotite granite that have a slab-like form. Importantly, it lacks metasedimentary xenoliths and is found only in contact with the subgranite or biotite granite. Some "ghost" xenoliths of biotite granite appear to be almost completely assimilated, suggesting the garnet granite represents late stage melting that has segregated completely from the source region and has intruded the adjacent subgranite and biotite granite.

LEUCOCRATIC GRANITE

The leucocratic granite is a coarse to medium grained K-feldspar-plagioclase-quartz granite, lacking significant amounts of biotite (2%) while containing some muscovite (2%), microcline feldspar (5%) and minor amounts of tourmaline and beryl. The leucocratic granite is seen as an undeformed intrusive in sequence 3 and as a faintly foliated margin of the garnet granite in sequence 1 (main map). The leucogranite also contains the odd 0.2 m - 1 m sized xenoliths of subgranite and biotite granite.

FELSIC GRANITE

The felsic granite is a strongly foliated, medium to coarse grained K-feldspar-plagioclase -quartz-muscovite-biotite granite. Table 1 gives the mineral proportions and shows that the biotite and plagioclase compositions are intermediate between the metasediments and the granites. The felsic granite occurs as a set of dyke like intrusions at Point Ellen, surrounded by extensively migmatised country rock. The K-feldspar megacrysts, not seen in the metasediment, crystalised as phenocrysts which overprint the foliation.

PEGMATITE

The pegmatites are a late stage feature, forming 1.5 m - 10 cm dykes that crosscut the layering and folding and occur with only minor variations within the field area. Generally, the

pegmatites are coarse to very coarse in grain size, and contain quartz, plagioclase, K-feldspar, muscovite, tourmaline (some tourmaline crystals approaching 30cm in length) and beryl. The grain size, mineralogy (tourmaline presence or absence, amount of quartz) or the contact relationships with the metasediments all vary in only a minor manner.

3.2. THE MIGMATITIC METASEDIMENTS

The metasediments are variously deformed and migmatised (these features are discussed in full in parts 4 and 5). They are characterised by a strong to moderate foliation and an often distinctive rodding lineation. The main mineral constituents are quartz, biotite, plagioclase, muscovite and rare K-feldspar, tourmaline and sillimanite. A subdivision is made on the basis of distinguishing the main mineral constituents in order to illustrate a general trend across the Vivonne Bay section (see section 5).

BIOTITE METASEDIMENT

The biotite metasediment is a dark, grey-black, well foliated biotite-plagioclase-quartz-muscovite metasediment that occurs only adjacent to the main granite bodies, the biotite and garnet granites of sequence 1 (main map). The biotite metasediment is characterised by titanium and iron rich biotites and calcium poor plagioclase feldspar. A distinctive feature of the biotite metasediment is the centimetre scale isoclinal folds. Quartz-feldspar layers are folded within a biotite-muscovite matrix possibly indicating the syn-deformational crystallisation of the melt phase (see section 4, migmatite fabric 4).

QUARTZ-BIOTITE METASEDIMENT

The quartz-biotite metasediment is a quartz rich (~ 40%) lithology, with a large proportion (~30%) of biotite and occurs in association with the melt bodies of sequence 1 (main map). Abundant quartz and plagioclase (~ 20%) porphyroblasts dominate the texture, obscuring a foliation which is not as penetrative as in the biotite metasediment. The dominance of quartz distinguishes this lithology from the biotite metasediment.

MUSCOVITE-BIOTITE METASEDIMENT

The muscovite-biotite metasediment is a muscovite-biotite-quartz-plagioclase metasediment with occasional distinctive layers containing clusters of muscovite. It is biotite rich (~30%) and is associated with the well migmatised (see section 4, migmatitic fabrics) zone of sequence 3 (main map). One example in this sequence contains 0.5 - 1 cm sized porphyroblasts of sillimanite altering to muscovite, indicating that the clumps, mentioned above, may have been smaller sillimanite crystals. This lithology is distinguished from the quartz-biotite metasediment by the dominance of the muscovite.

BIOTITE-QUARTZ METASEDIMENT

The biotite-quartz metasediment is found in sequence 3 and shows less migmatisation than the adjacent muscovite-biotite metasediment, is gently folded on the scale of metres, and is penetrated by leucocratic granite dykes. Containing the minerals, biotite (30%), quartz (30%) plagioclase (25%) and muscovite (15%), this metasediment is very similar to the muscovite-biotite metasediment . The titanium and iron contents of the biotites are low while the calcium content of plagioclase is high ($CaO \sim 7.3\%$) which is typical of the metasediments.

QUARTZ METASEDIMENT

The quartz metasediment is a medium grained quartz-plagioclase-biotite-K-feldspar metasediment. The quartz metasediment dominates the stratigraphy of the Point Ellen area (sequence 5, main map), and is characterised by biotite layers that define a strong foliation, and quartz elongations defining a distinctive rodding lineation. This metasediment becomes highly migmatised (see section 4) and hard to identify at the eastern margin of the sequence.

3.3. SUMMARY OF LITHOLOGICAL RELATIONSHIPS

The Vivonne Bay section displays some general trends. The metasediments become progressively more quartz rich away from the porphyritic granite. Biotite has high titanium and iron contents in the granites and biotite metasediment, and low contents in the other metasediments. Plagioclase is calcium rich in all rocks except the granites that appear to be intrusive.

The genetic association between the various granites and the metasediment and the use of overprinting criteria, allows the evaluation of a relative age sequence. From oldest to youngest; metasediment, porphyritic granite, subgranite, biotite-granite, garnet-granite, leucocratic granite/felsic granite with pegmatite occurring throughout the one event , but mainly as a late feature.

4. STRUCTURAL DESCRIPTION

4.1. DEFORMATION PHASES

Mapping the Vivonne Bay section has revealed five distinct phases of deformation. Evidence for these phases as well as their relative ages determined by overprinting criteria, are outlined in figure [2], illustrated in figure [3] and discussed below.

PHASE ONE DEFORMATION, D_1

The Vivonne Bay migmatitic metasediments have a generally northerly dipping, strong foliation defined by the alignment of biotite grains. This foliation is folded and sheared by all other deformations (Figure [3], sketch 1), and is interpreted as an early S_1 fabric developed during regional scale folding not observed on the scale of the coastal exposures (Figure [3], sketch 2). An unambiguous original S_0 bedding fabric was not seen in the field area, the high grade of the section having obliterated diagnostic evidence, although some possible relic crossbedding was observed in a few outcrops.

PHASE TWO DEFORMATION, D_2

Mesoscopic tight to isoclinal folding of the S_1 foliation throughout the Vivonne Bay section results in a S_2 axial planar foliation and S_1-S_2 intersection lineation, L_1 (Figure 3, sketch 1). These F_2 generally upright folds plunge west-south westerly or east-north easterly and are especially distinctive in the biotite metasediment of sequence 1 (Main map). However, the isoclinal folding of the biotite metasediment is defined by the quartz-plagioclase feldspar leucosome layers instead of the biotite foliation (Figure 3, sketch 3). The biotite defined folds are interpreted as occurring concurrent with a local compressive phase, while the leucosome defined folds are interpreted as being due to the process of layer dilation upon melt extraction from the biotite metasediment.

FIGURE 2 : DEFORMATION HISTORY OF THE VIVONNE BAY SECTION

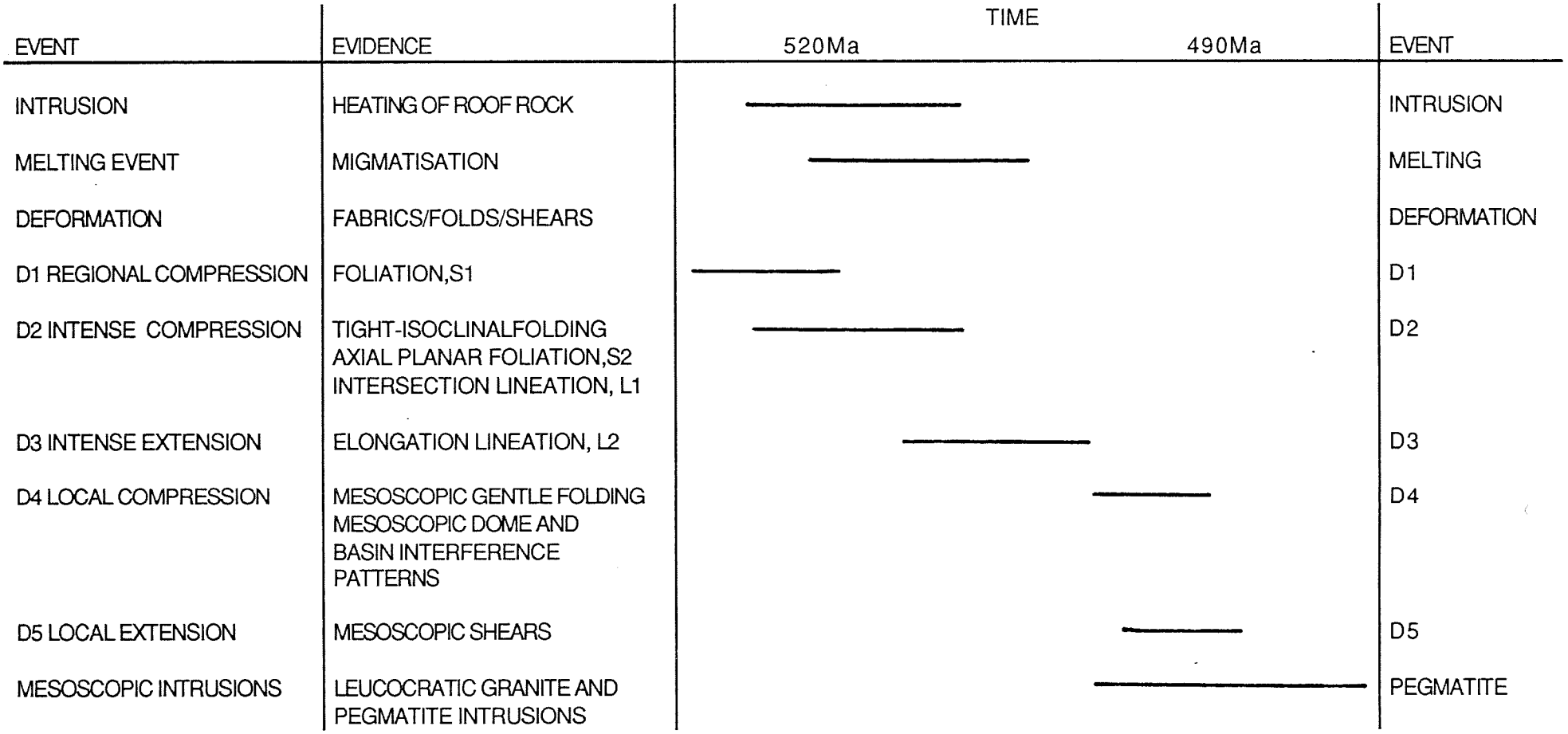

PLATE 1

Photographs of the migmatite fabrics and structural features of the Vivonne Bay section

Scale on the hammer is 10cm long.

a: Photograph of sheared metasediment with granitic melt confined to the shears and a few connecting layers, migmatite fabric 1.

b: Photograph of migmatite fabric 2 showing larger layers of melt and biotite accumulations.

c: Photograph of highly migmatised metasediment, fabric 3.

d: Photograph of folded leucocratic melt layers within a biotite rich metasediment, fabric 4.

e: Photograph of the D_2 isoclinal folds.

f: Photograph of the distinctive rodding lineation, at Point Ellen.

g: Photograph of a large xenolith slab of biotite granite (Bt.Gt.)within the garnet granite (Gnt. Gt.).

h: Photograph of the intrusive leucocratic granite (leuco.gt.)at the eastern end of sequence 3 that has migmatised its margin.

a

e

b

f

c

g

d

h

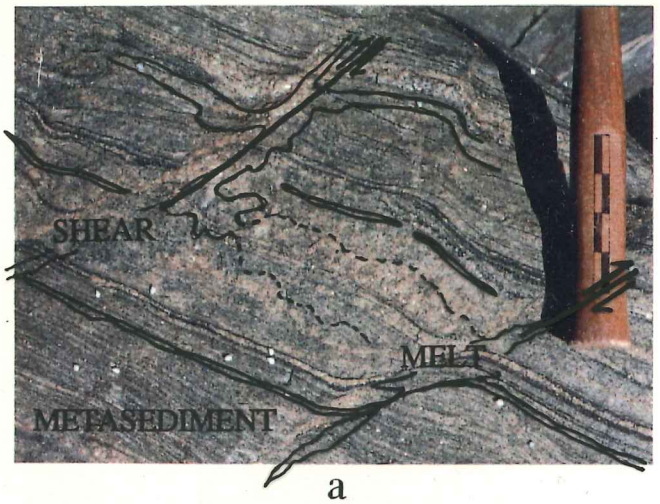
SHEAR
MELT
METASEDIMENT

a

e


MELT

b

f


RAFT
MELT

c

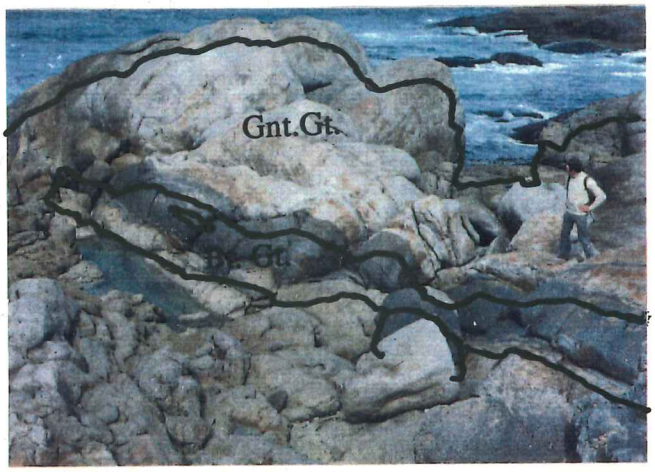
Gnt.Gt.
Gt.

g


MELT

d

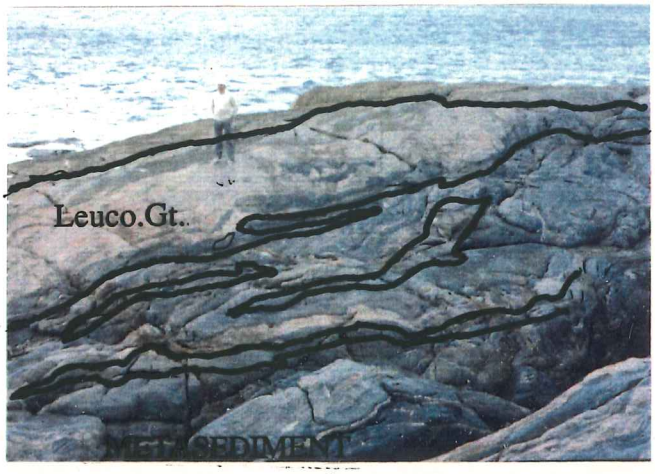
Leuco.Gt.

h

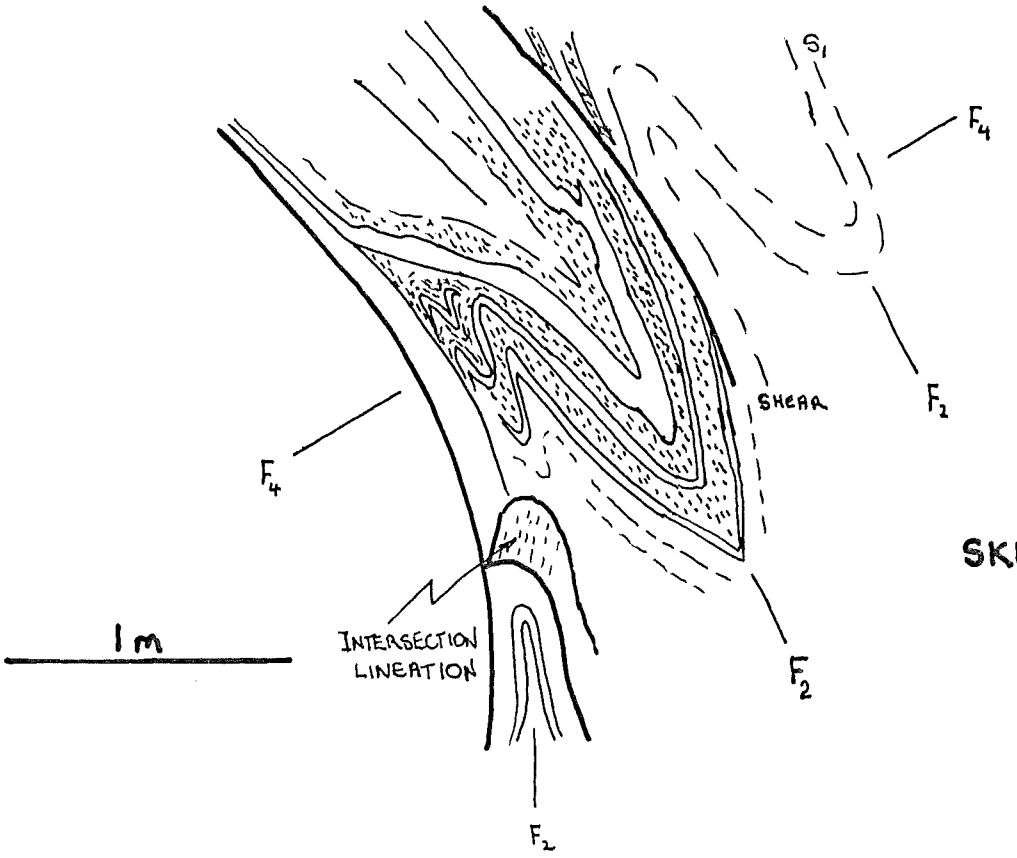

SKETCH 1

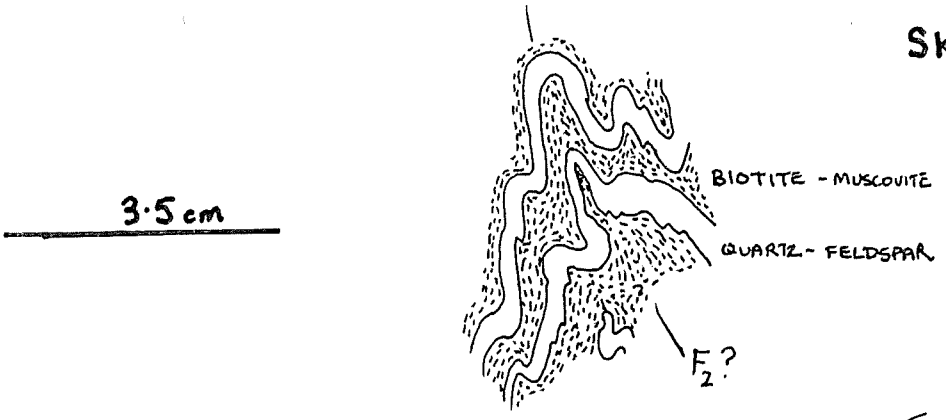

SKETCH 2

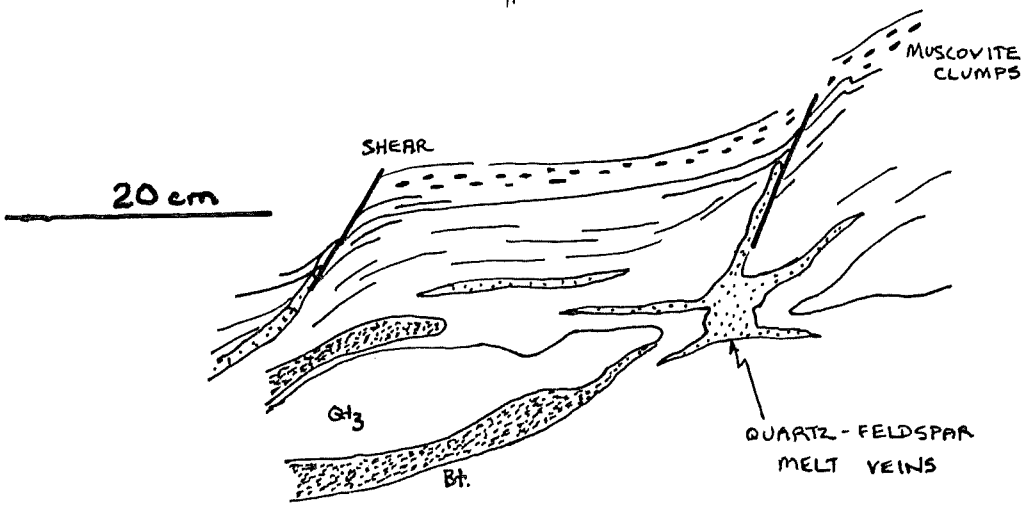

SKETCH 3

FIGURE [3]

PHASE THREE DEFORMATION, D_3

A third phase of deformation is indicated by the presence of a strong quartz-plagioclase mineral elongation lineation, L_2, within the migmatitic metasediments, especially the quartz metasediment of sequence 5 (main map). This lineation has a variable plunge, being folded by late mesoscopic gentle folds of phase four, but trends south-south westerly. The lineation is always approximately down dip and in the plane of the main foliation, S_1. The weathered surface of lineated metasediment produces a distinctive rodding profile (Plate 1, photo f).

PHASE FOUR DEFORMATION, D_4

The fourth phase of deformation involves mesoscopic gentle folding that appears mainly in sequence 3 and 5 (main map). The folding is distinctively harmonic, with a wavelength of between 1 to 25 metres, and occurs as two orthogonally orientated sets of fold axis that produce dome and basin interference effects. The two sets of fold axes are orientated approximately north-south and east-west, and in general have only gentle plunges of between 5 and 25°. This phase post dates the migmatisation event but coincides with localised melting due to the intrusion of pegmatites and leucocratic granite. D_4 also folds all other fold generations, hence this deformation phase is interpreted as occurring very late in the structural history.

PHASE FIVE DEFORMATION, D_5

Phase five deformation is characterised by shearing on three different scales. The shearing of entire 400-700m of outcrop cuts through all phases of folding, except D_4, and is associated with the pegmatite intrusive event. Many of the pegmatite veins have penetrated the metasediments along these shears. The scale of shearing can also be inferred by the sudden changes in the strain gradient as one proceeds along the coastline, from small scale shears to harmonic D_5 folds, then suddenly to sheared rock again.

The second set of mesoscopic shears occurs along length scales of 10m to 1m and involves minor adjustments associated with the late D_5 gentle folding. These shears also act as

focusing sites for pegmatitic intrusion, and hence they are interpreted as occurring during the late stage extensional phase.

The third set of shears occurs on the scale of foliated layers, in conjunction with the melting phase. This relationship is shown in figure [3], sketch 3 and plate 1, photo a.

4.2. MIGMATITIC FABRICS

The Vivonne Bay section has a diversity of migmatitic fabrics. The fabrics are composed of two components; the palaeosome, or melted fraction, and the neosome, the unmelted host rock. The diversity stems from different degrees of melting and their relationship to deformation.

FABRIC 1

This fabric has the palaeosome confined to 20-30 cm long shears and specific layers concordant with the main foliation (Plate 1, photo a). These shears often occur as *en echelon* sets resulting in offsets of the order of centimetres. The fabric is dominated by 5-10 cm wedges of foliated metasediment, with the small (1-10mm thick) granitic palaeosome layers having 2-3 mm thick biotite rims. This fabric is interpreted as an early stage, low melt fraction, migmatitic fabric. It is noteworthy that, even at this stage of melting, the granitic palaeosome is interconnected.

FABRIC 2

The amount of palaeosome is significantly greater in this fabric, with layers reaching up to 5cm thickness. The granitic palaeosome is often seen in concordance with the D_2 isoclinal folding alongside late veins that crosscut the foliation and folding (Plate 1, photo b). Biotite accumulations are also larger, forming up to 10 cm wide rafts. This fabric is interpreted as an intermediate stage of melting where neither neosome nor palaeosome dominates.

FABRIC 3

This fabric is dominated by the palaeosome, with a high proportion of contorted granitic veins interconnecting and forming distinct pods (Plate 1, photo c). Metasediment occurs as rounded xenoliths ranging in size from 5 to 25 centimetres. Deformation features are generally obscured at this level of migmatisation. This fabric is interpreted as a late stage of melting but before the palaeosome component has completely segregated to form metre scale regions of granite.

FABRIC 4

This migmatitic fabric is characterised by 1-2 cm wide veins of quartz - plagioclase - K-feldspar that are isoclinally folded within a very biotite rich (>35%) metasediment. The folding in fabric 2 is defined by a biotite foliation, while in this fabric it is defined by the palaeosome layers (figure [3], sketch [2]). Fabric 4 is found in both the biotite metasediment and subgranite (Plate 1, photo d). A possible explanation for this folding is the dilation of the metasedimentary layer upon melt extraction. This would indicate that the biotite metasediment is a residue rock, a possibility which is investigated in the geochemistry section.

4.3. SUMMARY OF STRUCTURAL DESCRIPTION

Five main phases of deformations have been distinguished on the basis of overprinting criteria. An initial S_1 foliation (D_1) is isoclinally folded (D_2) and subsequently stretched, resulting in a mineral elongation lineation (D_3) that is most distinctive in the unmelted metasediments. A later phase of gentle folds (D_4) and mesoscopic shears (D_5) occurs prior to small scale pegmatitic and leucocratic granite intrusions.

The metasediments have four main fabrics, illustrated, in order of increasing melting, in Plate 1, photomicrographs a, b, c and d. Fabric 4 has isoclinally folded palaeosome within a biotite rich host, that may represent an advanced stage of melt extraction.

The overprinting of initial compressive then final stretching forces is characteristic of forceful diapiric intrusion (Hibbard, 1986). At Vivonne bay there is an early compressive phase, indicated by isoclinal folding, followed by a stretching phase, resulting in a strong mineral elongation lineation. These two phases are interpreted as occurring concurrently with the intrusion of the porphyritic granite.

The leucocratic and garnet granite crosscut all deformations and appear to be very late stage intrusives. Pegmatite dykes are even later stage intrusives.

5. METAMORPHISM

5.1. MINERALOGY OF THE VIVONNE BAY SECTION

The mineral diversity of the Vivonne Bay section is not great. In particular, it lacks pressure-temperature sensitive mineral assemblages that would provide diagnostic information on the conditions of metamorphism. The mineral distribution along the Vivonne Bay section from west to east is shown in figure [4].

The Vivonne Bay section is dominated by the minerals quartz, sodic plagioclase, biotite and muscovite. K-feldspar is restricted to the granites and the leucosome component of the migmatites. Garnet is found only in late stage veins which crosscut the main garnet granite body (Plate 2, photo b) and a few small (1 metre wide) pegmatite dykes. Sillimanite porphyroblasts (Plate 2, photomicrograph a), that overgrow the dominant biotite foliation, are found in a few layers of metasediment at the western end of sequence 3. The layers in which sillimanite occurs are very biotite and muscovite rich (total ~70%), with little quartz and feldspar.

The distinction of metasediment lithologies is a simplification based on the main mineral components seen on a scale greater than ten metres. On a smaller scale (< 10 metres) the metasediments have highly variable amounts of quartz, plagioclase feldspar, biotite and muscovite. There is however, a general trend in the mineral composition of the metasediments; from a biotite and muscovite-biotite metasediment at the western end of the section,to the quartz dominated metasediment of Point Ellen at the eastern limit of the section.

The biotites of the metasediments are characterised by low titanium, high magnesium and low iron contents (Table 1). The granites are characterised by high titanium, low magnesium and high iron biotites (Table 1). This distribution is consistent with the granites containing predominantly residual biotites. Sodic plagioclase dominates the metasediments while the more calcic plagioclase is confined to the porphyritic and biotite granites (Table 1).

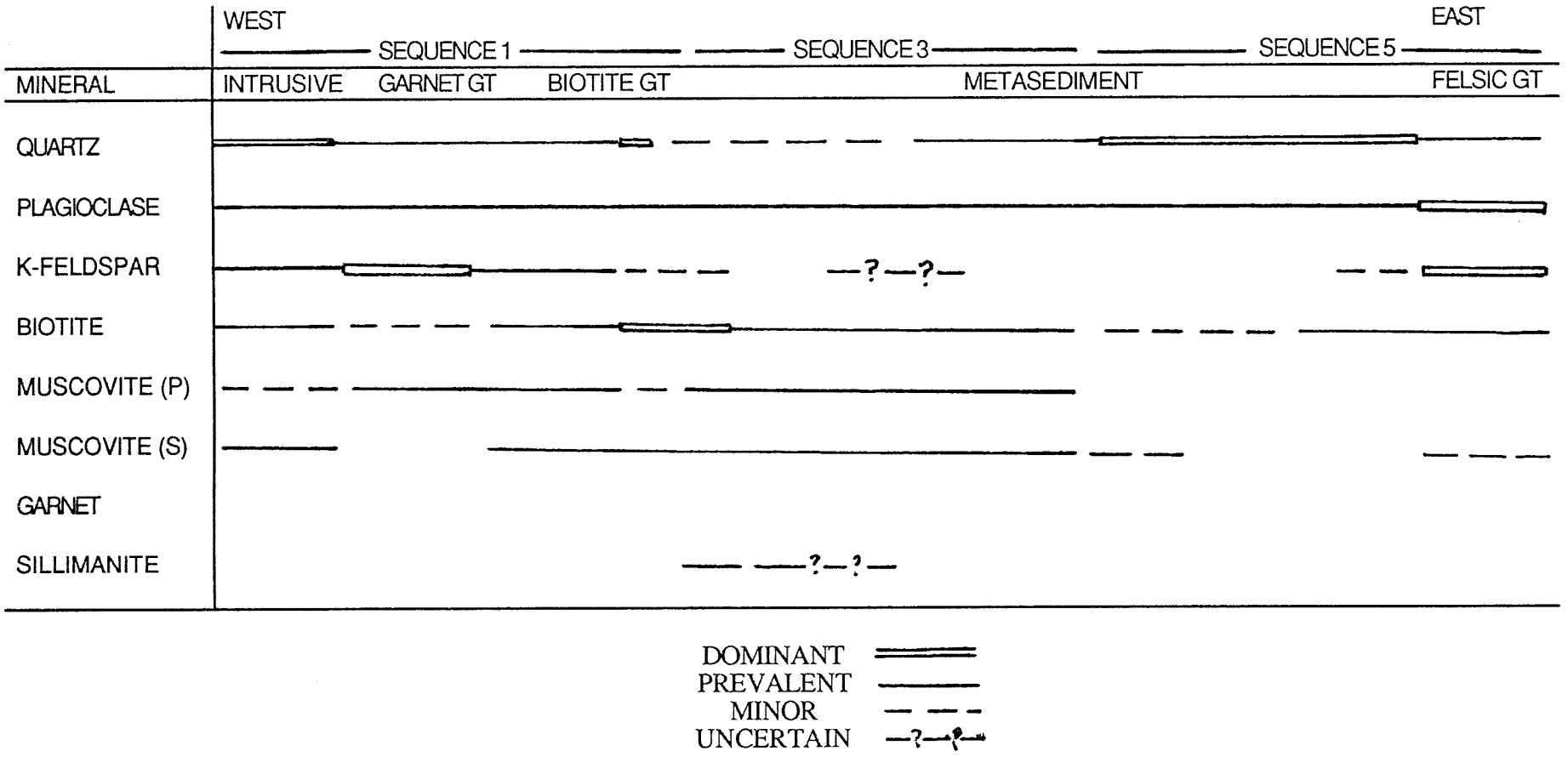

FIGURE [4] : MINERAL ASSEMBLAGES ACROSS A SIMPLIFIED SECTION OF VIVONNE BAY

TABLE 2. SELECTED MIGMATITE-GRANITE ANALYSES FROM VIVONNE BAY AND THE LACHLAN FOLD BELT

SAMPLE	1	2	3	4	5	6	7	8	9	10
SiO2	56.11	80.09	67.36	73.82	71.5	76.55	71.88	72.21	72	69.1
TiO2	0.8	0.24	0.7	0.45	0.46	0.04	0.51	0.46	0.54	0.55
Al2O3	19.04	9.9	14.67	12.31	13.31	13.61	13.59	13.42	13.72	14.3
Fe2O3T	8.01	1.63	5.3	3.55	3.71	0.36	3.22	3.06	4.07	3.96
MnO	0.12	0.02	0.08	0.06	0.06	0.01	0.05	0.05	0.06	0.06
MgO	4.33	0.59	2.82	1.58	1.67	0.19	1.34	1.16	1.76	1.82
CaO	1.1	0.54	2.24	1.68	1.84	0.55	1.66	1.5	0.95	2.49
Na2O	1.25	2.5	2.29	2.39	2.59	2.81	2.77	2.95	1.49	2.21
K2O	6.95	3.46	3.26	3.29	3.48	5.13	4.04	4.19	3.73	3.63
P2O5	0.14	0.07	0.18	0.08	0.07	0.2	0.23	0.24	0.13	0.13
Total	99.54	99.52	99.79	99.77	99.23	100.2	99.95	99.87	100	98.3
RATIO	1.644	1.12	1.524	1.167	1.17	1.218	1.137	1.107	1.67	1.18
TRACE ELEMENTS (ppm)										
Sr	188	172	198	149	155	19	154	154	127	139
Rb	248	111	160	164	158	153	207	208	153	180
Y	30	19	32	50	53	6.2	22	26	39	32
Zr	117	116	227	185	175	21	167	173	201	170
Nb	16	5.6	14	14	13	3.7	15	16	9	11
Pb	42	17	34	29	?	20	26	?	35	27
Th	15	8.2	15	18	?	2.3	11	?	22	19
U	3.4	3.1	5.4	4.8	?	1.8	2.4	?	4	3
Ga	22	9.8	19	15	?	16	17	?	15	17
Ba	2402	855	806	488	596	19	531	661	765	480
Sc	19	6	17	11	12	2	10	12	12	14
V	144	27	101	76	67	3	54	66	64	72
Cr	156	32	126	84	68	17	57	48	56	46
Ce	70	55	75	61	67	12	63	78	68	69
Nd	27	19	36	24	23	5	26	28	24	25
La	37	23	41	33	27	10	27	36	31	31
Ni	53	2	30	20	25	3	0	17	24	17

(1) Biotite metasediment, (Sample 929-05) (2) Quartz Metasediment, (Sample 929-17)
(3) Subgranite, (Sample 929-26) (4) Biotite Granite, (Sample 929-34)
(5) Biotite Granite, (Foden, 1989) (6) Garnet granite, (Sample 929-29)
(7) Porphyritic Granite, (Sample 929-07) (8) Porphyritic Granite, (Foden, 1989)
(9) Cooma Granodiorite, Lachlan Fold Belt (Chappell, 1984)
(10) Average of 316 analyses of S-type granites from the Lachlan Fold Belt (Chappell and White 1982)

Muscovite occurs both in primary and secondary forms. The primary muscovite is distinguished by it's subhedral crystal habit, concordance with the foliation, alteration of the edges to biotite and the often numerous biotite inclusions. The secondary muscovite is euhedral, unaltered and overgrows the foliation fabric of the biotites (Plate 2, photo a). The most spectacular example of secondary muscovite occurs as sillimanite alteration haloes (Plate 2, photo a). In general muscovite dominance follows a similar pattern to biotite, decreasing towards sequence 5. Muscovite is also seen associated with leucocratic veins within the metasediment and late veins within the garnet and leucocratic granites. This is evidence for muscovite occurring as a product of melting.

Myrmekitic textures, indicating late stage quartz-plagioclase intergrowth, are seen in most granites and the biotite metasediment (Plate 2, photo c). Sometimes the myrmekite is seen in the pressure shadow of larger plagioclase phenocrysts possibly indicating syn-deformational crystallisation of melt (Hibbard, 1986). This evidence is inconclusive however, since the foliation is often faint or non existent in most thin sections in which myrmekite occurs and it's relationship to the deformation unclear.

5.2. MIGMATISATION

The subgranite and some examples of the metasediment, particularly the biotite metasediment, have K-feldspar rich layers which display a granitic texture on the scale of a thin section (Plate 2, photo d). The granitic layers contrast well with the strongly foliated, biotite rich layers that display a more typical metasedimentary texture in thin section (Plate 2, photo d). The granitic layers are interpreted as leucosomes, or melt layers, while the foliated metasediment is interpreted as the residual component of melting.

The leucosomes are composed of the minerals quartz, plagioclase, K-feldspar and secondary muscovite. The metasediments are dominated by the minerals quartz, biotite, plagioclase and muscovite. The melting reaction must therefore describe the melting of the quartz-plagioclase-muscovite component of the metasediment while leaving behind a biotite

PLATE 2

Photomicrographs of thin section features of
the Vivonne Bay section

Width of view approximatly 3.5mm

a: Photomicrograph of the basal section of sillimanite (Sill) porphyroblasts (grey prisms) within a biotite (Bt)-muscovite (Mus) matrix.

b: Photomicrograph of garnets (Gnt) confined to a vein within the garnet granite. The margins of the garnets have iron rich biotite (Bt) and muscovite (Mus) grains

c: Photomicrograph of myrmekite (Myr) in the pressure shadow of the large plagioclase feldspar (Plg) grain in the porphyritic granite. Also note the presence of secondary muscovite (Mus) and tourmaline (Tor).

d: Photomicrograph of the subgranite texture contrast. The subgranite has metasedimentary layers characterised by aligned biotite (Bt) while the granite leucosomes display a contrasting granitic texture.

a

b

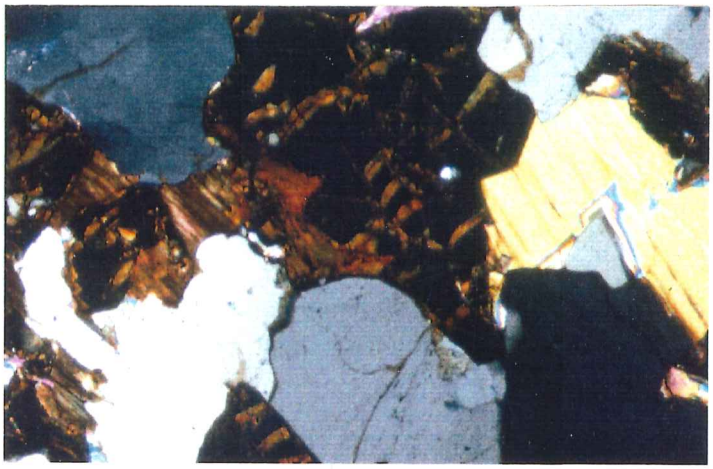

c

d

a

b

c

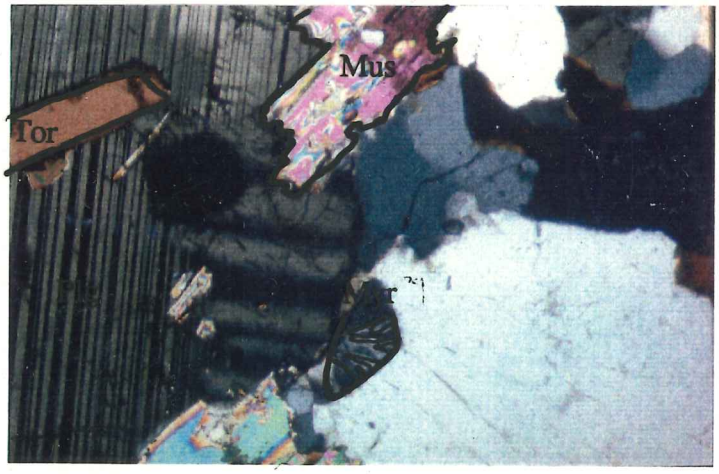

d

residue. The melt later crystalises K-feldspar, quartz and plagioclase. The initial melting reaction proposed is

$$\text{Muscovite} + \text{Quartz} + \text{Plagioclase} \rightarrow \text{Melt} + H_2O \quad (1)$$

$$\text{Melt} \rightarrow \text{K-feldspar} + \text{Quartz} + \text{Plagioclase} \quad (2)$$

The presence of lots of pegmatite dykes along the Vivonne Bay section, as well as the high proportion of secondary muscovite alteration within the metasediments, is an indication of the high levels of water present. This could complicate the actual melting reactions and, if the system is close to water saturation, the 'wet' granites may not migrate far from their source environment (White and Chappell, 1988). Muscovite breakdown described in (1) and (2) above occurs at about 700°C at 0.7 GPa given a vapour free melting environment (White and Chappell, 1988). If the temperature continues to increase to about 850°C at 0.7 GPa, then biotite will break down (White and Chappell, 1988). The melting reaction will be,

$$\text{Biotite} + \text{Quartz} + \text{Plagioclase} + \text{Melt} \rightarrow \text{Melt} + H_2O \quad (3)$$

White and Chappell (1988) also suggest that the muscovite breakdown will produce only small amounts of melt and migmatisation, while the biotite breakdown will produce enough melt to exceed the critical melt fraction (van der Molen and Paterson, 1979) and form homogeneous granite accumulations.

5.3. SUMMARY OF METAMORPHIC FEATURES

A quartz-plagioclase-biotite-muscovite metasediment has undergone initial heating, developing sillimanite in some layers. Further heating has seen muscovite break down in the first phase of melting. In the second phase, biotite begins to break down and upon crystallisation of the K-feldspar -quartz-plagioclase melt, excess water from biotite and muscovite is flushed through the rock pile. Biotite is predominantly a residual mineral, while secondary muscovite is favoured in the water rich environment. This raises the possibility that

the biotite metasediment may be the residue from the melting of the original metasediment, producing a biotite granite.

The porphyritic granite of the Vivonne Bay section has a high concentration of granites at its margin and the metamorphic grade reduces, in a general sense, from this core to Point Ellen. This indicates that the porphyritic granite was the source of the heat that produced the local melting.

6. GEOCHEMISTRY

6.1. OBJECTIVES

The objectives of the geochemical section are to test some of the interpretations of the previous sections. For example:

(1) The residual nature of the biotite metasediment

(2) The late-stage nature of the garnet granite

(3) The intrusive nature of the porphyritic granite

(4) The genetic relationship between the biotite granite and biotite metasediment.

This section of work will also investigate the possibility of a genetic link between the granites and enable the modeling of the processes involved. Furthermore, the S-type nature of the Vivonne Bay granites is determined as well as a comparison with a classic S-type terrain, the Lachlan Fold Belt (L.F.B.). The advantage of the Vivonne Bay section is that, unlike the L.F.B., we can see direct melting relationships between granite and source which we can confirm through the geochemical analyses.

6.2. GEOCHEMISTRY OF THE GRANITE-MIGMATITE

6.2.1. INTRODUCTION

Geochemical analyses were performed in order to further define the relationship between the Vivonne Bay granites and the metasediment. The results of the major and trace element analyses, as well as the isotope analyses, are summarised in Table 2. To compare with examples from other regions, analyses of the Cooma Granodiorite (Chappell 1984) and an average value for the Lachlan Fold Belt (Chappell and White 1982) have been included. The results of the analyses are graphically displayed in figures [5], [6] and [7]. Included in the

graphs of figures [5] and [6] are the analyses of the Remarkable Rocks granite and Cape Willoughby granite from the south coast of Kangaroo Island.

6.2.2. CLASSIFICATION OF THE VIVONNE BAY SECTION GRANITES AND COMPARISONS WITH THE L.F.B.

The analyses of the granites and migmatites can be classified into two general groups. The first group, which includes the garnet granite, Remarkable Rocks granite, Cape Willoughby granite and to a lesser extent the high silica examples of the porphyritic granites and biotite granites, is relatively high in silica ($SiO_2 > 71\%$), potassium ($K_2O > 4\%$) and sodium ($Na_2O > 3.2\%$) and relatively low in magnesium ($MgO < 1.5\%$), iron ($Fe_2O_3T < 3\%$, where Fe_2O_3T is the total Fe measured as Fe_2O_3) and most trace elements such as Sr, Ga and Zr (Figures [5] and [6]).

The second group includes the Lachlan Fold Belt granites, biotite granite, subgranite and biotite metasediment. Group 2 are characterised by lower silica ($SiO_2 < 7.1\%$) and potassium ($K_2O < 4\%$) and high titanium ($TiO_2 > 0.4\%$), calcium ($CaO > 1.5\%$) and most trace elements, for example, Sc, V and Cr (Figures [5] and [6]).

The Lachlan Fold Belt (L.F.B.) S-type (see 6.1.3.) granites are well known for their relationship with a sedimentary source (White and Chappell 1988). Sample 10, Table 2, shows the averaged major and trace element analyses of 316 S-type granites from the L.F.B. (Chappell and White 1982), which are also plotted on the figure [5] and [6] graphs. Also in Table 2 is an analyses of the Cooma Granodiorite, a specific example from the L.F.B. suite.

The L.F.B. granites plot between the subgranite and biotite granite analyses. The composition of the averaged analyses is comparable with the group 2 granites, having lower silica (SiO_2 ~ 69-70%) than the group 1 Remarkable Rocks and Cape Willoughby granites.The fact that the L.F.B. granites have a composition close to the subgranite and biotite granite is consistent with the Vivonne Bay examples being similar metasediment derived granites.

FIGURE 5: MAJOR ELEMENT CHEMISTRY

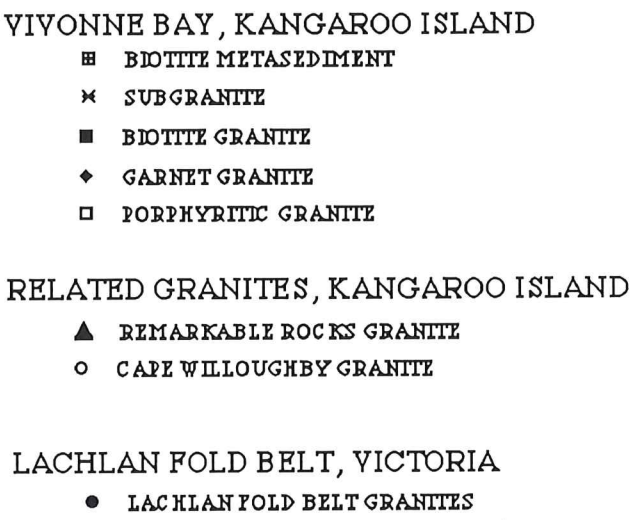

Remarkable rocks granite from Foden, 1989
Cape Willoughby granite from Foden, 1989
Lachlan Fold Belt Granites are an average of 316 S-type granite analyses from Chappell and White, 1982

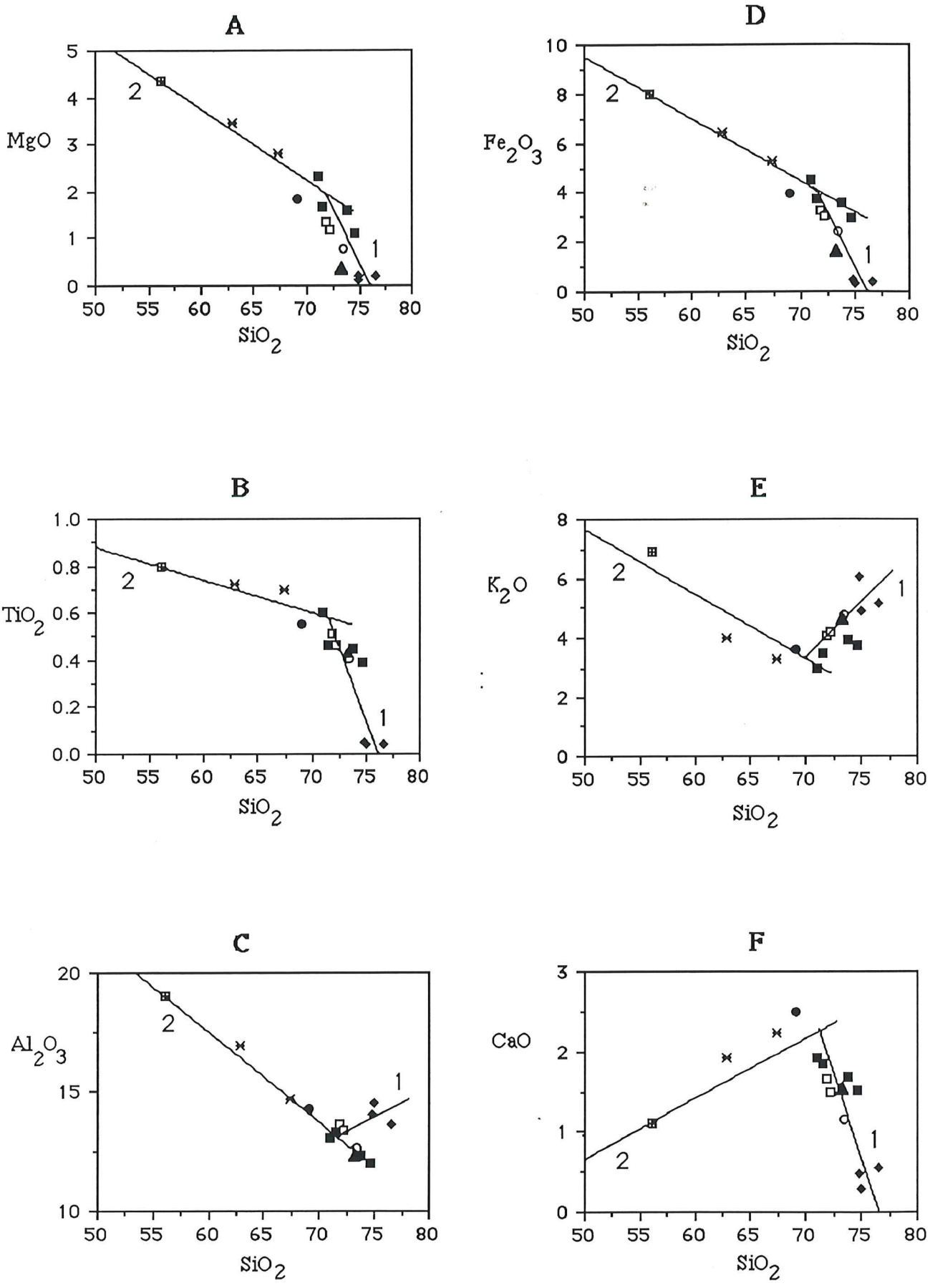
A
MgO
SiO2
B
TiO2
SiO2
C
Al2O3
SiO2
D
Fe2O3
SiO2
E
K2O
SiO2
F
CaO
SiO2
1
2

FIGURE 5

FIGURE 6: TRACE ELEMENT CHEMISTRY

VIVONNE BAY, KANGAROO ISLAND

- ⊞ BIOTITE METASEDIMENT
- ✕ SUBGRANITE
- ■ BIOTITE GRANITE
- ◆ GARNET GRANITE
- □ PORPHYRITIC GRANITE

RELATED GRANITES, KANGAROO ISLAND

- ▲ REMARKABLE ROCKS GRANITE
- ○ CAPE WILLOUGHBY GRANITE

LACHLAN FOLD BELT, VICTORIA

- ● LACHLAN FOLD BELT GRANITES

Remarkable rocks granite from Foden, 1989
Cape Willoughby granite from Foden, 1989
Lachlan Fold Belt Granites are an average of 316 S-type granite analyses from Chappell and White, 1982

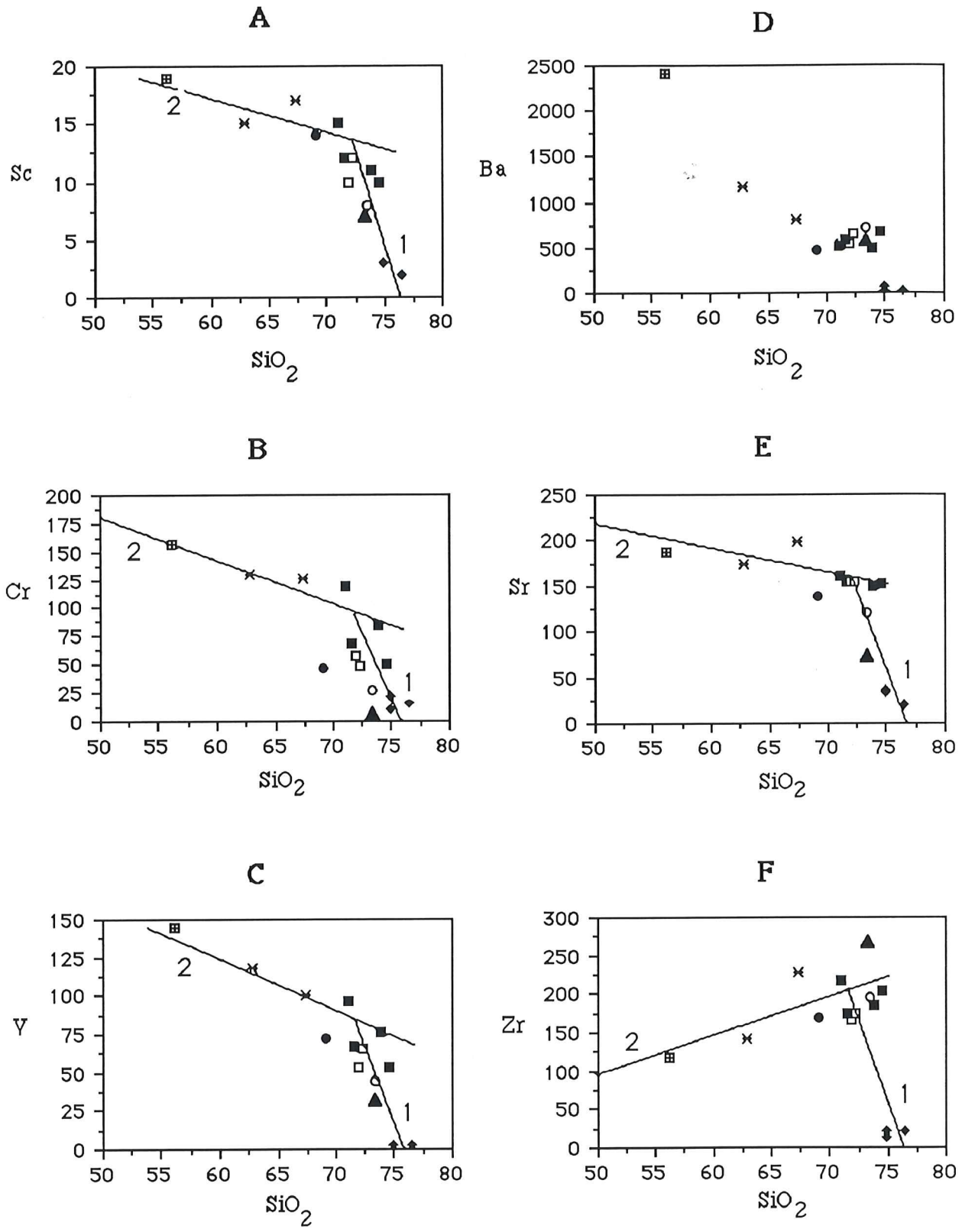
A
Sc
20
15
10
5
0
50 55 60 65 70 75 80
SiO2
2
1
D
Ba
2500
2000
1500
1000
500
0
50 55 60 65 70 75 80
SiO2
B
Cr
200
175
150
125
100
75
50
25
0
50 55 60 65 70 75 80
SiO2
2
1
E
Sr
250
200
150
100
50
0
50 55 60 65 70 75 80
SiO2
2
1
C
Y
150
125
100
75
50
25
0
50 55 60 65 70 75 80
SiO2
2
1
F
Zr
300
250
200
150
100
50
0
50 55 60 65 70 75 80
SiO2
2
1

FIGURE 6

The Cooma Granodiorite, a classic S-type, has a composition that is very similar to the porphyritic granite of the Vivonne Bay section. This similarity suggests that the porphyritic granite is also a product of melting of the metasediments. The most noticeable difference is that the porphyritic granite is higher in potassium and sodium and lower in total iron (table 2).

6.2.3. S-TYPE GRANITE TEST

Chappell and White, 1974, suggest a number of possible parameters that characterise the S-type and I-type granites. The chemical erosion of a sedimentary sequence will result in the fractionation of sodium into seawater and calcium into carbonates (Chappell and White 1974). The sediment is also relatively enriched in aluminium and thus when acting as a source region for granitic melts will impart these chemical characteristics distinguishing the melts as S-type (Chappell and White 1974). One of the most diagnostic parameters is the amount of aluminium compared with the amount of sodium, potassium and calcium. Therefore, this can be expressed as a molar ratio such that :

$$\text{RATIO} = \text{MOL}\left(\frac{Al_2O_3}{Na_2O+K_2O+CaO}\right) \qquad > 1.1 \text{ for S-types}$$

$$< 1.1 \text{ are I-types}$$

Table 2 shows this value for each sample, including the L.F.B. averaged analyses, and indicates that, at least by this test, all rocks are S-type. There appears to be a decreasing trend in this ratio , or reducing S-type character, from the metasediments (RATIO ~ 1.6), subgranite (RATIO ~ 1.5) and biotite granite (RATIO ~ 1.2) down to the marginal porphyritic granite (RATIO ~ 1.1). Other geochemical data such as the isotope analyses may further refine the argument.

6.2.4. SOME GENERAL TRENDS

On the major and trace element graphs each group that was described in section 6.1.2 appears to have its own linear trend, as indicated by the lines marked 1 and 2 (Figures [5] and [6]). Line 1, which relates the high silica granites, connects the porphyritic granite to the garnet

[6]). Line 1, which relates the high silica granites, connects the porphyritic granite to the garnet granite,and includes the Remarkable Rocks and Cape Willoughby granites at an intermediate stage. This trend is interpreted as a fractionation line and will be tested by geochemical modeling in sections 6.4.2. and 6.4.3. Line 2, which relates the low silica granites of group 2, joins the biotite metasediment and subgranite to the biotite granites, porphyritic granite and the L.F.B. granites.

The biotite metasediment has a high proportion of Al, K, Na, Mg (low silica) and most trace elements. For example, the trace elements Ba, V and Sc, all of which are retained by the biotite residue in a melting system, are found in relative abundance in the biotite metasediment. On this basis the biotite metasediment can be interpreted as representing a residue after melt has been extracted from the metasediment sequence. The biotite metasediment also forms the low-silica, or residual, end of the trend line 2.

The subgranite appears to have an intermediate geochemical character between the biotite metasediment and biotite granite. The subgranite analyses plot at about the midpoint of line 2 (Figures [5] and [6]) contain 63 - 67% SiO_2 and are relatively high in magnesium (MgO ~ 3.0%), iron (Fe_2O_3T ~ 6%), titanium (TiO_2 ~ 0.7%) and most trace elements, for example Sc,V and Ba.

Line 2, which connects the residual biotite metasediment to the subgranite and subsequently to the biotite granite, is interpreted as a partial melt mixing line. This suggests that the subgranite approximates the bulk composition of the original melting metasediment before significant melt segregation, while the biotite granite is the result of the accumulation of melt extracted from the metasediment.

The two trend lines are approximately connected in the biotite granite -porphyritic granite region. The porphyritic granite forms the silica rich limit of group 2 and line 2 and the silica poor limit of group 1 and line 1. The implication of this is that the porphyritic granite represents the most evolved member of the mixing trend (Line 2) while also acting as the source

for the fractionated melts (Line 1). In almost all analyses the porphyritic granite plots in the same general area as the biotite granite, implying a related source region.

6.3. ISOTOPE ANALYSES

The continental crust has a distinctive geochemical signature brought about by the fractionation trends associated with melt segregations from the mantle. A consequence of this is that the crust will develop, over time, different and characteristic Sr and Nd isotopic systematics from the increased contribution for the decay of Rb and Sm. This provides reservoirs that will result in melts with characteristic isotopic signatures. Analysis of the isotopic compositions of the Vivonne Bay granites and a typical metasediment can give us some clues as to the origin of the melts.

The results of the isotope analyses are shown in Table 3 and presented diagramatically in Figure [7a] and [7b]. The Sr^{87}/Sr^{86} data plotted against Rb^{87}/Sr^{86} in Figure [7a] defines an isochron which gives an age of 521+/- 10 Ma (Model 3, Isochron Basic Program, Foden 1989) for the melting event with an initial Sr^{87}/Sr^{86} ratio of ~ 0.72. This compares well with the age data of inrusives into the Kanmantoo Group, for example, 516+/- 5 Ma age for the Rathjen Gneiss (zircon ion probe age , Foden *pers. com.*). It is important to note that the strontium isotope data must be viewed with caution, since it is not clear, *a priori*, that complete isotopic homogenization occurred at the time of melting. However some support for the notion of homogenization at 521 Ma is indicated by the fact that the calculated Sr^{87}/Sr^{86} ratios at 521 Ma are all ~ 0.72 (Table 3).

Both chondritic and present day ε_{Nd} values are presented in Table 3 and the present day ε_{Nd} is plotted against depleted mantle Nd model age in Figure [7b]. Included are other analyses of S-type, I-type and mafic rocks of the Adelaide Fold Belt (Foden *pers. com.*). The mafic rocks have generally high ε_{Nd} and a spread of model ages, while the I-type granites have similar ε_{Nd} levels but youger model ages (Figure [7b]). The Vivonne Bay section S-type granites plot at very low ε_{Nd} and old model ages. The plot has a linear trend, marked line 3, suggesting a

TABLE 3. ISOTOPE DATA FOR THE VIVONNE BAY SECTION

sample no. (see below)	1	2	3	4	5
Nd ppm	17.43	19.77	31.2	4.72	44.09
2 sigma error	0.01	0.01	0.01	0.01	0.01
Sm ppm	3.64	4.32	5.7	1.115	9.1
2 sigma error	0.01	0.01	0.01	0.01	0.01
143/144 Nd	0.511716	0.511788	0.511689	0.51197	0.511791
2 sigma error	0.000035	0.000035	0.000035	0.000035	0.000035
Sm/Nd	0.209	0.219	0.183	0.236	0.206
147Sm/144Nd	0.126	0.132	0.111	0.143	0.125
143/144Nd chur	0.512638	0.512638	0.512638	0.512638	0.512638
143/144Nd dep. mantle	0.513114	0.513114	0.513114	0.513114	0.513114
Model Age (CHUR)	2.05	2.07	1.72	1.97	1.85
Model Age (Dep. Mantle)	2.22	2.24	1.94	2.20	2.07
Eps. Nd (present day)	-17.99	-16.58	-18.51	-13.03	-16.52
age (T)	0.52	0.52	0.52	0.52	0.52
143/144(T)	0.51129	0.51134	0.51131	0.51148	0.51137
143/144 (Chur at T)	0.51198	0.51198	0.51198	0.51198	0.51198
Eps Nd (w.r.t. Chur at T)	-13.47	-12.45	-12.94	-9.61	-11.91
Sr87/86	0.74	0.74748	0.7329	0.89617	0.74404
Average 2 sigma error	0.0001	0.0001	0.0001	0.0001	0.0001
Sr ppm	152.17	154.10	170.57	18.50	146.53
Rb ppm	151.86	205.16	109.43	152.07	162.97
Rb/Sr	0.998	1.331	0.642	8.220	1.112
87/86(T)	0.71858	0.71890	0.71913	0.71974	0.72017

(1) Biotite granite, sample from Foden (1989).

(2) Porphyritic granite, sample 929-07.

(3) Quartz metasediment, sample 929-17.

(4) Garnet granite, sample 929-29.

(5) Biotite granite, sample 929-34.

FIGURE 7

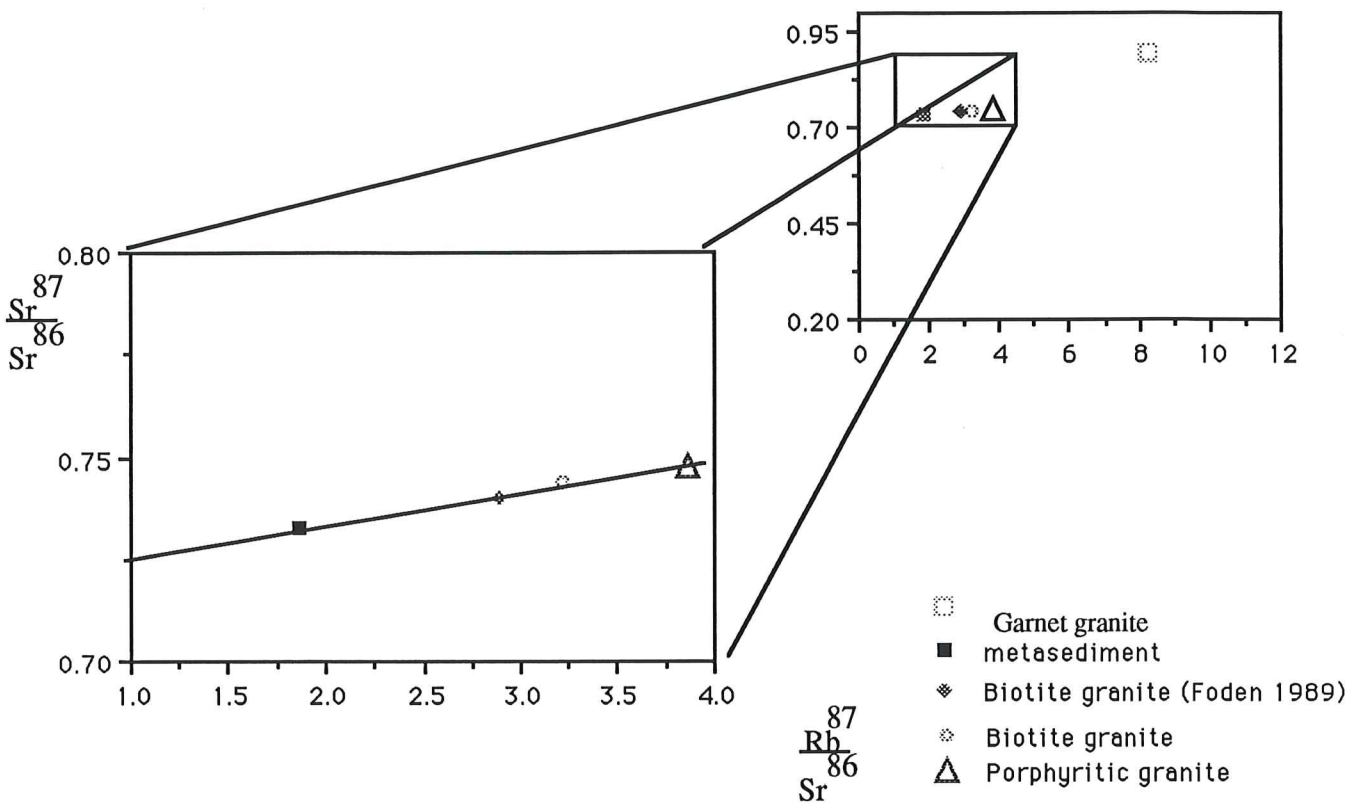

7 a) Rb/Sr ISOTOPE RESULTS

Isochron defining an age of 521 +/- 10 Ma for the Vivonne Bay migmatisation phase

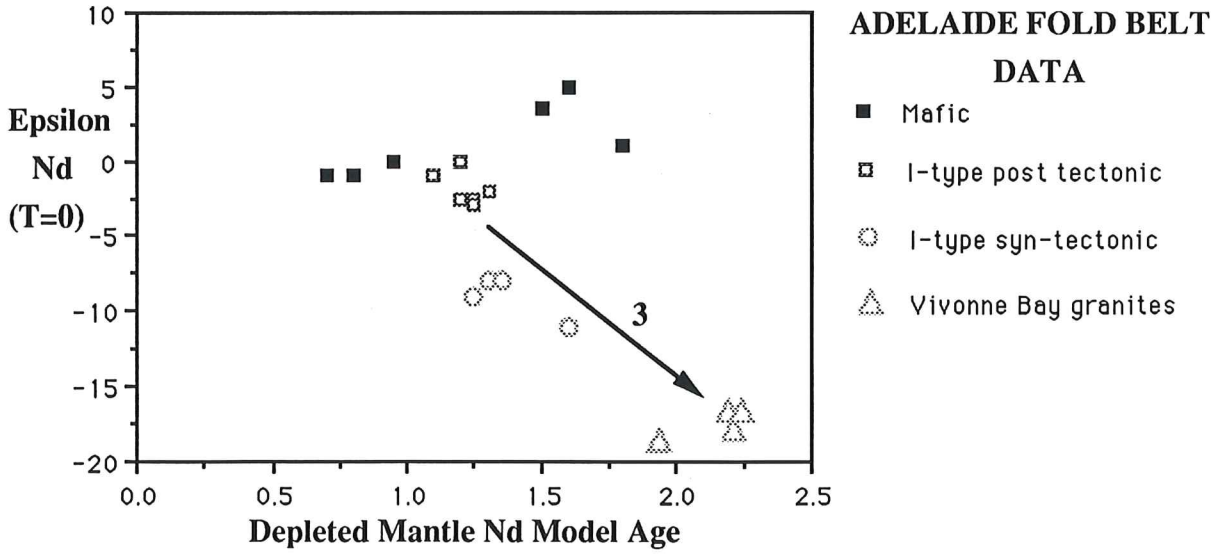

7 b) Nd isotope results

Plot of Present day epsilon Nd against depleted mantle Nd model age for various Adelaide Fold Belt melts

(Mafic and I-type data from Foden, *pers. comm.*)

genetic relationship between mafic rocks and I-type granites on one hand and S-type granites and ancient crust on the other.

Ancient crust has very low ε_{Nd} values ($\varepsilon_{Nd} < -20$) and very old model ages (> 2.5 Ga) and this will likely be reflected in the characteristics of an S-type granitic melt. The I-type granites reflect mantle source regions and hence have isotopic compositions similar to the mafic rocks (Foden, pers. comm.). These I-type granites may contribute to the generation of S-type melts as they move to higher levels of the crust, and will pass on some of their isotopic character.

6.4. GEOCHEMICAL MODELING

6.4.1. PARTIAL MELTING OF THE METASEDIMENTS

The linear trend expressed by line 2, relating the biotite metasediment, subgranite and biotite granite, represents a partial melt mixing line. This relationship can be used to estimate the degree of melting of the metasediments that has produced the biotite granite. This partial melting model treats the biotite metasediment as a residue and the biotite granite as the extracted melt. For the purposes of this exercise, the subgranite is assumed to approximate the composition of the unsegregated partially melted metasediments.

Application of the lever rule to the bulk rock trace element composition in the following manner

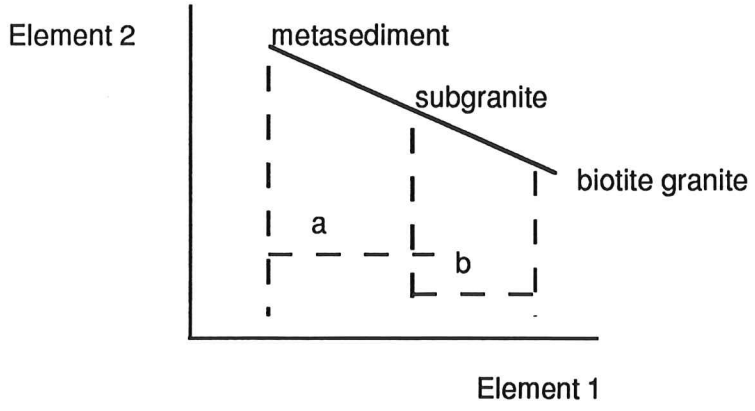

$$\% \text{ biotite granite in subgranite} = a * \frac{100}{a+b}$$

enables the resolution of the percentage of biotite granite in the subgranite. A mixing line mass balance basic program developed on this principle by Foden, 1989, resulted in a 60% level of melting of the subgranite required to produce the biotite granite. This degree of melting was consistently generated for most of the different trace elements, reinforcing the partial melting interpretation.

6.4.2. MASS BALANCE TEST

The proposed fractionation of the porphyritic granite or biotite granite to produce the garnet granite, as expressed by the linear trend of line 1 in the figures [5] and [6], can be modeled on the basis of mass balance. Expressed simply, the mass balance of a fractionating system is:

100% of Rock A = y% of Rock B + x% of crystals.

[PARENT] [DAUGHTER] [RESIDUE]

For the Vivonne Bay section the equation becomes:

Porphyritic granite = y% Garnet granite + x% residual minerals

or, alternatively:

Biotite granite = y% Garnet granite + x% residual minerals.

The composition of the crystalised minerals are the phenocrysts seen in the parent rock and for this model they are quartz, plagioclase feldspar, biotite and apatite. Petrographic evidence suggests that the K-feldspar megacrysts are the product of the melting. To keep errors to a minimum the K-feldspar was therefore excluded from the model residue. Mineral compositions are taken from microprobe data while the compositions of the biotite granite, porphyritic granite and garnet granite are taken from the X.R.F. data sets of Table 2.

TABLE 4

1) Least-squares model for garnet granite (1) with porphyritic granite (2) as parent.

	1	2	Crystals	Fraction	Proportion of residue(%)
SiO_2	76.55	71.88	Quartz	0.183	36
Al_2O_3	13.61	13.59	Plag. An17	0.172	33.9
$Fe_2O_{3(t)}$	0.36	3.22	Biotite	0.149	29.3
MnO	0.01	0.05	Apatite	0.004	0.7
MgO	0.19	1.34			
CaO	0.55	1.66	Garnet granite	0.497	49.70%
Na_2O	2.81	2.77			
K_2O	5.13	4.04	% Crystalisation		50.30%
TiO_2	0.04	0.31			
P_2O_5	0.2	0.23	Sum of $(residuals)^2$		0.0048

2) Least-squares model for garnet granite (1) with biotite granite (3) as parent.

	1	3	Crystals	Fraction	Proportion of residue(%)
SiO_2	76.55	73.82	Quartz	0.273	39.6
$Al2O_3$	13.61	12.31	Plag. An17	0.225	32.6
Fe_2O_3	0.36	3.55	Biotite	0.189	27.4
Mno	0.01	0.06	Apatite	0.002	0.29
MgO	0.19	1.58			
CaO	0.55	1.68	Garnet granite	0.314	31.40%
Na_2O	2.81	2.39			
K_2O	5.13	3.29	% Crystalisation		68.60%
TiO_2	0.04	0.45			
P_2O_5	0.2	0.08	Sum of $(residuals)^2$		0.0393

TABLE 5

Specific solution to trace element distribution during fractionation.

Trace Element	C_i Porphyritic granite	D	Calculated C_l Garnet granite	Analysed X.R.F. Garnet granite
Sr	154	1.794	88.8	19
V	54	5	3.37	3
Nd	26	1.039	25.3	5
Sc	10	3.52	1.74	2
Cr	57	2.9	15.27	17
Ba	531	1.545	363	19

The fractionation trend was tested using the least-squares model of Bryan *et al.*, 1969, and the results listed in Table 4. The first set of results (Table 4.1) model the derivation of the garnet granite from the porphyritic granite. A measure of the error, the sum of the squared residues, is very low (~0.005) for this test, suggesting a good result. The model predicts that the porphyritic granite composition is equivalent to 50% residual minerals and 50% garnet granite.

The second set of results (Table 4.2) models the derivation of the garnet granite from the biotite granite. The sum of squared residues is again very low but not as good as the first model. This second model suggests the garnet granite is the result of 31% fractionation of the biotite granite, leaving 69% residual crystals. Due to the very low error of the first model, the 50% fractionation of the porphyritic granite is favoured.

6.4.3. TRACE ELEMENT DISTRIBUTION TEST

The previous mass balance test has predicted a level of fractionation and residual crystal composition necessary to produce the garnet granite from the porphyritic granite. The trace element distribution within the residue and melt can be modeled based upon the relationship

$$\frac{C_l}{C_i} = F^{(D-1)}$$

where C_l is the concentration of trace element in liquid, C_i is the initial concentration of trace element in parent rock, F is the % fusion, and D is the bulk distribution co-efficient.

Considering the garnet granite fractionation from the porphyritic granite, the C_i and D are known, while the previous section modeled a 50% fusion level (Table 4 model 1). Therefore we can solve for C_l and compare the results with the known concentrations in the garnet granite from the X.R.F. analyses (Table 2). The results of these calculations and the comparable X.R.F. results are listed in Table 5. The trace elements Ba, Sr, V, Sc,Nd and Cr were chosen because they are not as sensitive to zircon and apatite concentrations as are other

elements. In particular the trace elements Ba, V and Sc are heavily partitioned to biotite and model well.

The results show that V, Sc and Cr model very well but Sr, Nd and Ba less so. This could be due to a number of factors, especially the choice of bulk distribution coefficients which effect the solution critically.

The above approach is a specific solution for a given degree of fractionation (50%). The basic program Fractional Crystallisation Residues (Foden, 1990) models trace element compositions for melt and residue for different levels of fractionation (10% intervals, 10%-80%),and provides a more general solution that is sensitive to the distribution co-efficient chosen. The results of this program are shown in the graphs of figure [8], with the circles representing actual Vivonne Bay section examples. The upper line displays the evolution of the liquid component, while the lower line represents the residual component, with each cross showing solutions for 10% fractionation increments.

The results show Cr and V modeling very well, with Sc and Ba less so but still consistent with the overall trend. The results reinforce the notion that the garnet granite is a fractionated product of the porphyritic granite.

Figure 8 : TRACE ELEMENT DISTRIBUTION MODEL RESULTS

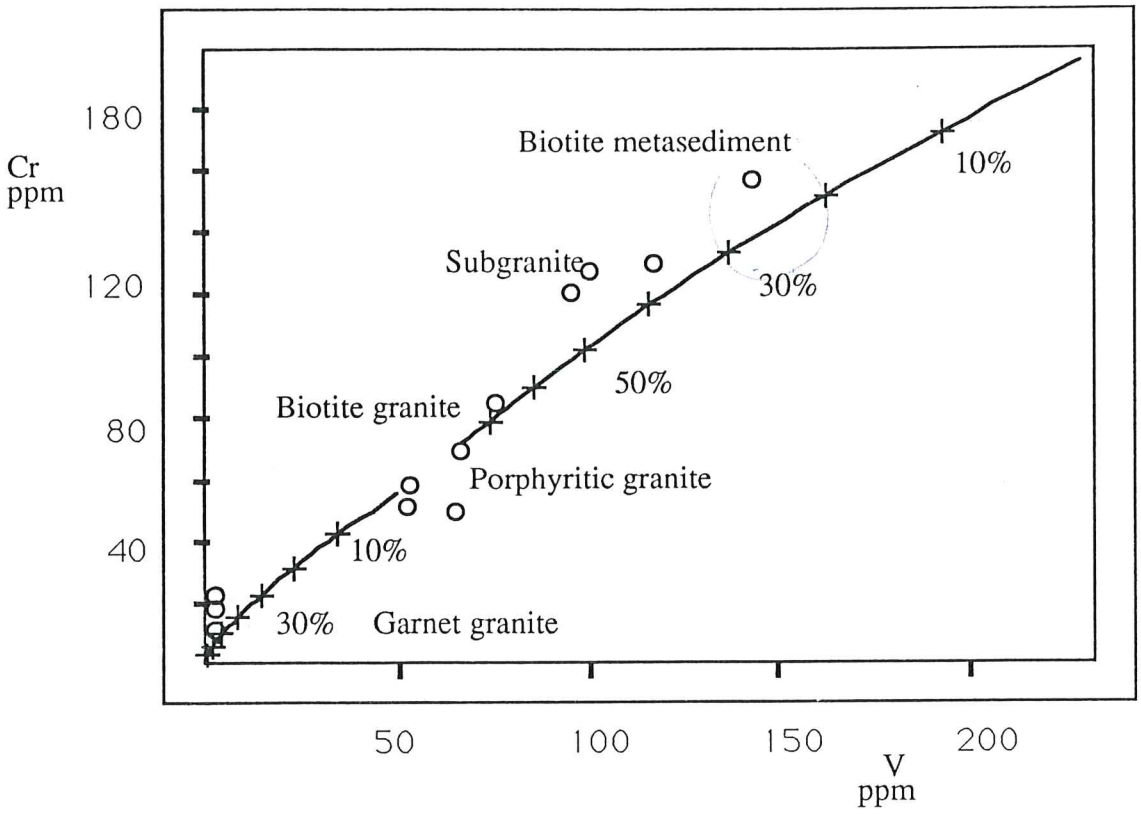

Figure 8A: Porphyritic Granite source with 54 ppm V and 57 ppm Cr with Kd V =4.4 and Kd Cr =3.3.

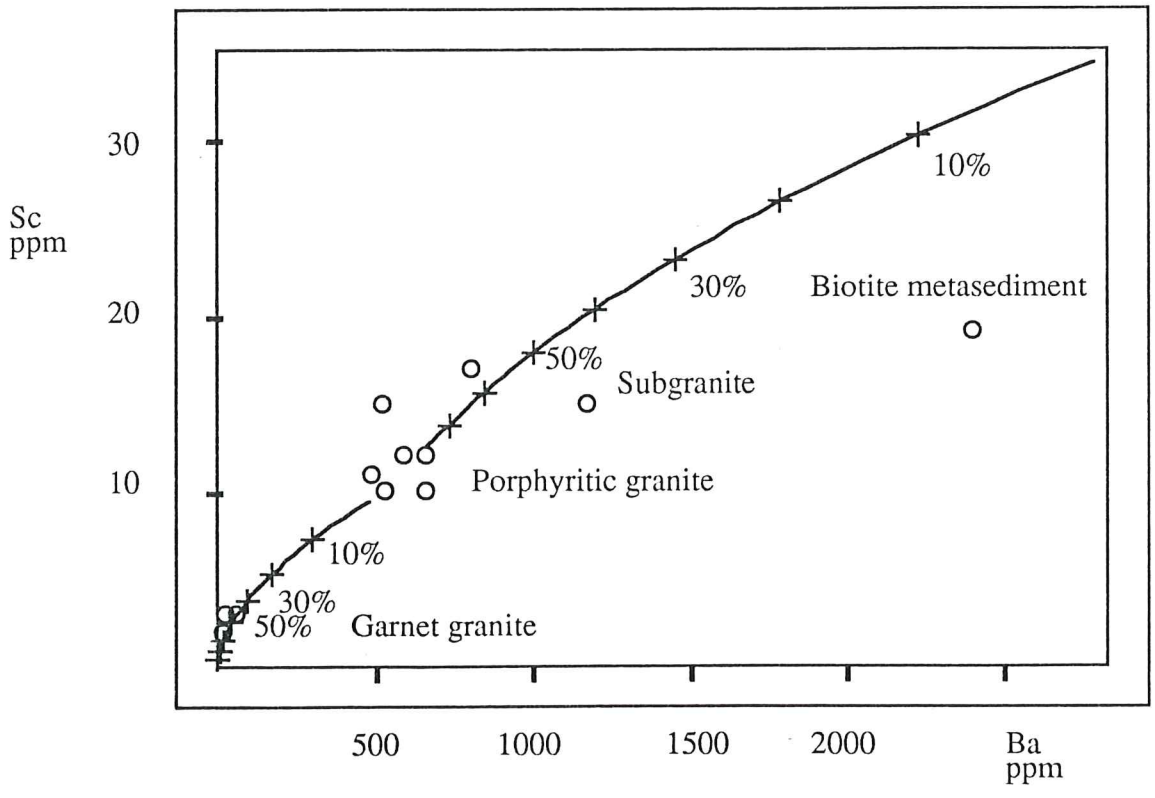

Figure 8B : Porphyritic granite source with 531 ppm Ba and 10 ppm Sc with Kd= 4.5 for Ba andKd= 3.52 for Sc.

7. INTERPRETATION AND CONCLUSIONS

Two major trends are evident from the geochemical analyses. The first trend, associated with the biotite metasediment, subgranite, biotite granite and porphyritic granite, defines a partial melting mixing trend. A simple mass balance test suggests that the biotite granite is the result of 60% melting of a metasediment that has a composition equivalent to the subgranite. This partial melting model defines the biotite metasediment as the residual component of the sequence.

The second trend, associated with the porphyritic granite and garnet granite, defines a fractionation line. The other Kangaroo Island granites, the Cape Willoughby and Remarkable Rocks granites, also lie on this fractionation trend. The garnet granite is interpreted as a product of fractionation from the porphyritic granite. Mass balance models and the trace element distribution test reinforce this conclusion.

The granites of the Vivonne Bay section therefore represent different stages of melt evolution. The first stage is indicated by the subgranite, with abundant granitic veins within a metasediment matrix, and is clearly a unsegregated partial melt. The second stage produced the biotite granite which is a segregated partial melt (60%) derived from the metasediments that has not moved a significant distance from the source region and can be considered relatively in-situ. The porphyritic granite is the third stage of granite evolution representing a homogeneous pluton scale accumulation of second stage melts This is indicated by the strong geochemical association between the porphyritic granite and the garnet granite. The field relationships and the petrographic differences suggest the porphyritic granite is an intrusive that has migrated some distance from the source region. The fourth stage of melt evolution is the generation of garnet granite by fractionation from the porphyritic granite. The highly depleted geochemical composition of the garnet granite indicates it is a small melt fraction segregation that has evolved at a relatively late stage, and subsequently intruded the metasediment.

The porphyritic granite forms the core of the Vivonne Bay section, with the degree of metamorphism inversely proportional to the distance from the pluton. Most of the other granites occur directly on the plutons margins, especially the biotite granite, which has formed in-situ as a result of partial melting of the metasediments. All of these factors indicate that the porphyritic granite was the source of heat that migmatised the metasediments.

Diapiric ascent of the porphyritic granite is likely to have taken place under stoping and roof rock melting mechanisms. Stoping is indicated by the highly evolved nature of the pluton, requiring rapid ascent of the magma, while the roof rock melting mechanism is indicated by the highly contaminated S-type composition as well as the S-type granite aureole that occurs at it's margin at Vivonne Bay. The dyke like offshoots of leucocratic granite result in small scale migmatisation, and may contribute to the overall emplacement mechanism for the pluton, as regions of the roof rock are weakened and finally completely melted.

In conclusion, it is evident that:

1. Pluton scale accumulations of S-type granite occur as a porphyritic granite at Vivonne Bay, the geochemistry and field relationships enabling the linking of this granite to the genesis of the other granites in the section, either as fractionation products or the result of partial melting.

2. The most definite S-type granite at Vivonne Bay, the biotite granite, shows intimate genetic relationships with the host metasediment and is the result of partial melting. Segregation of the melt component has occurred only on a small scale and the granite is relatively in-situ.

3. The garnet granite is a product of fractionation from the porphyritic granite.

4. S-type granites can form by the thermal perturbation provided by a granitic intrusion, at least as a small scale(100's metres) aureole.

ACKNOWLEDGEMENTS

Mike Sandiford is thanked for providing the opportunity to do this project and for the stimulus he provided as my original supervisor. John Foden is thanked for helping me beyond the call of duty and for taking on the role of supervisor late in the year.

Thanks also go to the technical staff of the Department of Geology and Geophysics, including Wayne Mussared, Geoff Trevelyan, Rick Barrett, John Stanley and Sherry Proferes. Huw Rosser of the Electron Optical Centre is thanked for his assistance with the electron microprobe.

A special thank you goes to Simon Turner who provided tremendous support and some excellent advice when the going got tough. Thanks also go to Kurt Stuwe for demonstrating infinite (finite differences approximation?) patience with a bothersome Honours student. Kathy Stewart, Peter Dymoke, Bunge, Graham Moss, Martin Kennedy and Jo Arnold are thanked for their support and friendship. A big thank you goes to my fellow Honours students for their sense of good fun and for putting up with me most of the time. The Jerry Cornelius of time, Geoff Fraser, is thanked for his friendship and for agreeing with me some of the time.

I would also like to thank Sarah Mitchell for her encouragement and for making me laugh a lot. I am indebted to Tim Reade and Tom Fung for the great friendship and the financial support they have given.

I am extremely grateful to both Mum and Dad for providing support throughout the year and for generally making life easier. Finally, thanks go to Jan Gardner, for all that cooking, and a huge thank you goes to Trudi Gardner, who helped me so much it is hard to imagine how I would of done it without her.

REFERENCES

Arzi, A.A., Critical Phenomena in the Rheology of Partially Melted Rocks, *Tectonophysics*, **44**, 173-184, 1978.

Atherton, M.P. and Gribble, C.D. (Eds), Migmatites melting and metamorphism, Shiua Publishing Limited, U.K. 1983.

Atherton, M.P. and Tracy, J. (Eds), Origin of granite batholiths: geochemical evidence, Shiua Publishing Limited, U.K. 1979.

Bryan, W.B., Finger, L.W. and Chayes, F, Estimating proportions in petrographic mixing equations by least squares approximation. *Science*, 163, 426-427, 1969.

Bulau, J.R. and Waff, H.S., Mechanical and thermodynamic constraints on fluid distribution in partial melts. *Journal of Geophysical Research*, **84**, 6102-6107, 1979.

Chappell, B.W. and White, A.J.R., Two contrasting granite types. *Pacific Geology* **8**, 173-174, 1974.

Chappell, B.W., Source rocks of I- and S-type granites in the Lachlan Fold Belt, south-eastern Australia. *Phil. Trans. R. Soc. Lond.*, **A310**, 693-707, 1984.

Clark, G.L. and Powell, R., Basement-cover interaction in the Adelaide Fold Belt, South Australia: the development of an arcuate fold belt. *Tectonophysics*, **158**, 209-226, 1989.

Clemens, J.D. and Wall, V.J., Controls on the mineralogy of S-type volcanic and plutonic rocks. *Lithos*, **21**, 53-66, 1988.

Clemens, J.D. and Wall, V.J., Origin and evolution of a peraluminous silicic ignimbrite suite: the Violet Town Volcanics. *Contrib. Mineral. Petrol.* **88**, 354-371, 1984.

Daily ,B., Milnes,A.R., Twidale, C.R. and Barne, J.A., Geology and geomorphology. In Tyler, M.J., Twidale,C.R. and Ling J.K. (Eds), Natural history at Kangaroo Island. p 1-38, Royal Society of South Australia, Adelaide 1979.

Etheridge, M.A., Wall V.J. and Vernon, R.H., The role of the fluid phase during regional metamorphism and deformation. *J. Metamorphic Geol.*, **1**, 205-226, 1983.

German, R.M., The Contiguity of Liquid Phase Sintered Microstructures, *Metall. Trans*,**16A**,1247-1260,1985.

Hibbard, M.J., Deformation of incompletely crystallised magma systems: Granitic gneisses and their tectonic implications. *Journal of Geology*, **95**, 543-561, 1986.

Hildreth, W. Gradients in silicic magma chambers: Implications for lithospheric magmatism. *Journal of Geophysical Research*, **86**, 10153-10192, 1981.

Hine, R., Williams, T.S., Chappell, B.W. and White, A.J.R., Contrasts between I- and S-type granitoids of the Kosciusko Batholith. *J. of Geol. Soc. of Australia*, **25(4)**, 219-234, 1978.

Huppert, H.E. and Sparks, R.S., Chilled margins in igneous rocks. *Earth and Plan. Sci. Lett.*, **92**, 397-405, 1989.

Huppert, H.E. and Sparks, R.S., Melting the roof of a chamber containing a hot, turbulently convecting fluid. *J. Fluid Mech.*, **188**, 107-131, 1988a

Huppert, H.E. and Sparks, R.S., The generation of granitic magmas by intrusion of basalt into continental crust. *J. of Petrology*, **29**, 599-624, 1988b.

Jenkins, R, Level III Tectonics excursion to the Southern Mount Lofty Ranges and Kangaroo Island. Unpublished excursion notes, University of Adelaide,S.A. 1989.

Jurewicz,S.R., Watson, E.B., The distribution of partial melt in a granitic system:The application of liquid phase sintering theory, *Geochim. Acta*, **49**, 1109-1121, 1985.

Limb, N.J., A petrological and geochemical investigation of the granitic rocks of Kangaroo Island, South Australia. Unpublished Honours thesis, The Flinders University of South Australia. 1975.

Mancktelow, N.S., The structure and metamorphism of the southern Adelaide fold belt. Unpublished Phd thesis, Univ. Adelaide, 1979.

McKenzie, D., The extraction of magma from the crust and mantle, *Earth. Plan. Sci. Lett.*, **74**, 81-91, 1985.

Miller, C.F, Watson, E.B., Harrison, T.M., Perspectives on the source, segregation and transport of granitic magmas, *Trans. Roy. Soc. Edin.*, **79**, 135-156, 1988.

Milnes, A.R., Compston,W. and Daily, B., Pre- to syn-tectonoic emplacement of early Palaeozoic granites in south-eastern South Australia , *J. of Geol. Soc. of Australia,* **24**, 87-106, 1977.

Milnes, A.R., The Encounter Bay Granites, South Australia, and their environment. vol I&II Unpublished PhD thesis, University of Adelaide, S.A., 1973.

Niemi, A.N., Courtney, T.H., Settling in solid-liquid systems with specific application to liquid phase sintering, *Acta Metall.*, **31/9**, 1393-1401, 1983.

Oxburgh, E.R. and McRae, T., Physical constraints on magma contamination in the continental crust: an example, the Adamello Complex. *Phil.Trans. R. Soc. London*, **310**. 457-472, 1984.

Phillips, G.N., Wall, V.N. and Clemens, J.D., Petrology of the Strathbogie Batholith: A cordierite-bearing granite. *Canadian Mineralogist,* **19**, 47-63, 1981.

Van der Molen, I., Interlayer material transport during layer-normal shortening. Part 1. The Model, *Tectonophysics*, **115**, 275-295, 1985a.

Van der Molen, I., Interlayer material transport during layer-normal shortening. Part 2. Boudinage, pinch and swell and migmatite at Sondre Stromfjord Airport, West Greenland, *Tectonophysics*, **115**, 275-295, 1985a.

Van der Molen, I., Paterson, M.S., Experimental Deformation of Partially-Melted Granite, *Contrib. Mineral. Petrol.*, **70**, 299-318, 1979.

Watson, E.B., Brenan, J.M., Fluids in the lithosphere, 1.Experimentally -determined wetting characteristics of CO2-H2O fluids and their implications for fluid transport, host-rock physical properties, and fluid inclusion formation, *Earth Plan. Sci. Lett.*, **85**, 497-515, 1987.

White, A.J.R and Chappell, B.W., Some supra-crustal (S-type) granites of the Lachlan Fold Belt. *Trans. R. Soc. of Edin: Earth Sci.*, **79**,161-181, 1988.

White, A.J.R., Clemens, J.D., Holloway J.R., Silver, L.T., Chappell, B.W. and Wall, V.J., S-type granites and their probable absence in southeastern North America. *Geology*, **14**, 115-118, 1986.

Wickham, S.M. and Oxburgh, E.R., Low pressure regional metamorphism in the Pyrenees and its implication for the thermal evolution of rifted continental margins *Phil.Trans.R.Soc.Lond.*, A**321**, 219-242, 1987

Wickam, S.M., The segregation and emplacement of granitic magmas, *J. Geo. Soc. Lond.*, **144**, 281-297, 1987.

VIVONNE BAY MIGMATITE–GRANITE

M.N.

10m 30m 50m
20m 40m

SEQUENCE 5

M.N.

10m 30m 50m
20m 40m

SEQUENCE 1

M.N.

10m 30m 50m
20m 40m

SEQUENCE 1

M.N.

10m 30m 50m
20m 40m

SEQUENCE 3

LEGEND

SOIL/VEGETATION
SAND/BOULDER
CALCRETE
SHELLY LAYER
META-SEDIMENT
QUARTZ
MUSCOVITE-BIOTITE
BIOTITE-QUARTZ
QUARTZ-BIOTITE
BIOTITE

CLIFFTOP
CLIFF BOTTOM
COAST LINE
GEOLOGICAL BOUNDARY
MAJOR SYNCLINE/ANTICLINE WITH PLUNGE
SYNCLINE/ANTICLINE INFERRED
SHEAR FAULT
VERTICAL SHEAR
OUTCROP EDGE

LOCALITY

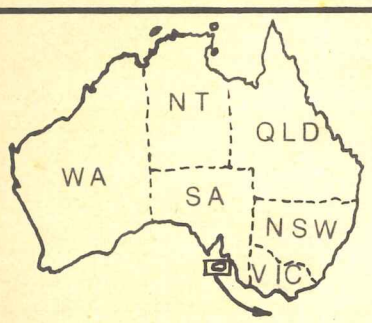

AUSTRALIA

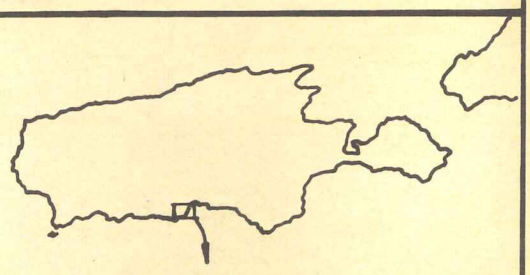

KANGAROO ISLAND